

When Are RL Hyperparameters Benign? A Study in Offline Goal-Conditioned RL

Jan Malte Töpperwien^{* 1} Aditya Mohan^{* 1} Marius Lindauer^{1,2}

Abstract

Hyperparameter sensitivity in Deep Reinforcement Learning (RL) is often accepted as unavoidable. However, it remains unclear whether it is intrinsic to the RL problem or exacerbated by specific training mechanisms. We investigate this question in offline goal-conditioned RL, where data distributions are fixed, and non-stationarity can be explicitly controlled via scheduled shifts in data quality. Additionally, we study varying data qualities under both stationary and non-stationary regimes, and cover two representative algorithms: HIQL (bootstrapped TD-learning) and QRL (quasimetric representation learning). Overall, we observe substantially greater robustness to changes in hyperparameter configurations than commonly reported for online RL, even under controlled non-stationarity. Once modest expert data is present ($\approx 20\%$), QRL maintains broad, stable near-optimal regions, while HIQL exhibits sharp optima that drift significantly across training phases. To explain this divergence, we introduce an inter-goal gradient alignment diagnostic. We find that bootstrapped objectives exhibit stronger destructive gradient interference, which coincides directly with hyperparameter sensitivity. These results suggest that high sensitivity to changes in hyperparameter configurations during training is not inevitable in RL, but is amplified by the dynamics of bootstrapping, offering a pathway toward more robust algorithmic objective design.

1. Introduction

The performance of deep reinforcement learning (RL) algorithms is notoriously sensitive to hyperparameter configurations. Small changes in, for example, learning rates,

target-update settings, or sampling choices can dramatically shift performance, so extensive hyperparameter tuning is frequently required to achieve competitive results (Henderson et al., 2018; Andrychowicz et al., 2021; Agarwal et al., 2021; Eimer et al., 2023; Becktepe et al., 2024; Farebrother and Castro, 2024). A second, subtler difficulty is that configurations that work early in training may become suboptimal later (Jaderberg et al., 2017; Parker-Holder et al., 2020), suggesting that the optimal regions of hyperparameters can vary over the course of learning (Mohan et al., 2023). These observations motivate a fundamental question that remains difficult to answer from standard RL training runs: *Is hyperparameter sensitivity intrinsic to RL, or do particular training mechanisms amplify it?*

Answering this in standard *online* reinforcement learning is difficult because exploration and optimization are entangled. Online agents must simultaneously (i) learn from self-generated data under imperfect exploration, and (ii) optimize objectives whose targets change as value estimates evolve. This coupling obscures whether the sensitivity to hyperparameters, previously studied predominantly in online RL (Eimer et al., 2021; Zhang et al., 2021; Parker-Holder et al., 2022; Eimer et al., 2023; Obando-Ceron et al., 2024), reflects an inherent property of the learning problem or if it arises from the interaction between tuning, exploration, and bootstrapping.

In this work, we utilize *offline goal-conditioned RL (GCRL)* (Foster and Dayan, 2002; Schaul et al., 2015; Andrychowicz et al., 2017; Ma et al., 2022; Ghosh et al., 2023; Park et al., 2025a) as a controlled setting to disentangle these factors. Offline GCRL offers two precise controls that standard RL lacks: (i) **Fixed Distributions:** By removing online exploration, we isolate the optimizer’s sensitivity to the data distribution from the agent’s ability to gather data (Levine et al., 2020). (ii) **Standardized Objectives:** Goal-reaching replaces complex reward shaping with a universal signal, allowing us to fairly compare diverse learning rules, from bootstrapped TD learning to supervised representation learning, on the exact same task structure. This setting allows us to treat data quality (e.g., expert vs. exploratory trajectories) as a controlled independent variable rather than a chaotic outcome of training.

¹Leibniz Universität Hannover ²L3S Research Center. Correspondence to: Jan Malte Töpperwien <m.toepperwien@ai.uni-hannover.de>, Aditya Mohan <a.mohan@ai.uni-hannover.de>.

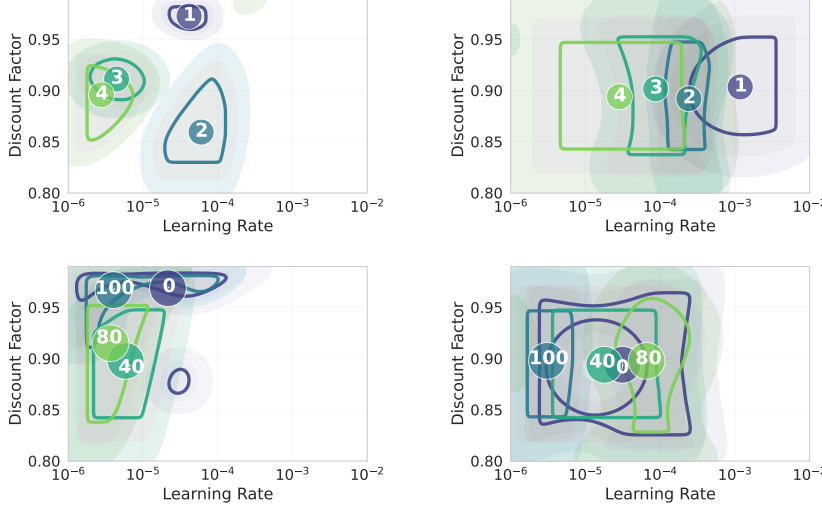


Figure 1. Isolation of objective sensitivity to hyperparameter configuration changes. By using offline GCRL, we isolate how learning mechanisms respond to data quality without the confound of exploration noise. We visualize the near-optimal region (top-10%) in the learning-rate – discount-factor plane (HIQL on the left and QRL on the right). **Top:** Scheduled training phases (1 → 4) with improving data quality. **Bottom:** Fixed offline mixtures at different quality levels. Even when data is fixed (offline), the bootstrapped method (HIQL) exhibits significant landscape drift, whereas the representation learning method (QRL) remains stable.

We analyze two methods that instantiate contrasting objectives in offline GCRL: (i) **HIQL** (Park et al., 2023), which learns a goal-conditioned value function with bootstrapped (TD) backups and then performs hierarchical policy extraction for long-horizon control (Park et al., 2025b); and (ii) **QRL** (Wang et al., 2023), which learns a quasimetric distance-to-goal objective (Myers et al., 2025a; Zheng et al., 2025; Myers et al., 2025b) without bootstrapping. To isolate the role of data quality under a fixed evaluation task, we construct controlled offline datasets that interpolate between expert demonstrations and exploratory trajectories. We additionally study *scheduled datasets* that shift from exploratory to expert-like data across training phases to introduce controlled training-time non-stationarity without changing the environment.

Across stationary and scheduled regimes, we perform extensive hyperparameter sweeps and characterize the resulting landscapes (performance as a function of hyperparameter configurations) using (i) *response surfaces*, i.e., low-dimensional slices of performance over hyperparameter pairs; (ii) *ε -optimality mass*, which measures the volume of near-optimal configurations; and (iii) *phase-resolved fANOVA profiles* (Hutter et al., 2014), which quantify which hyperparameters matter at each training stage. Our results reveal a consistent qualitative pattern: Hyperparameter landscapes for both types of objectives in offline GCRL are substantially more benign than landscapes in online RL during training (Mohan et al., 2023), even with degraded data quality. However, within this generally robust setting, a sharp divergence emerges (see Figure 1). Although QRL maintains broad, stable near-optimal regions once modest expert content is present, HIQL exhibits sharper optima and significant phase-to-phase reorganization, particularly under scheduled shifts. This demonstrates that sensitivity can persist, even when exploration is fixed, under certain combi-

nations of objectives and data non-stationarity. To explain this gap, we measure inter-goal gradient interference. We find that HIQL suffers from significantly stronger destructive interference than QRL, a diagnostic that correlates with the observed landscape drift. This suggests that an interplay between bootstrapped targets and shifting data distributions creates destructive gradient interference, a dynamic that may help explain the observed hyperparameter sensitivity.

Contributions. Our contributions are threefold: (i) We provide a systematic analysis of hyperparameter landscapes in offline GCRL across two representative algorithms, HIQL and QRL; (ii) We show that while offline landscapes are generally benign, bootstrapped (HIQL) and non-bootstrapped (QRL) methods exhibit distinct profiles of sensitivity to changes in hyperparameter configurations under data quality shifts; and (iii) We link the difference in the sensitivity profile to inter-goal gradient interference, motivating testable hypotheses about why certain training objectives are more sensitive to distribution shifts.

2. Preliminaries

In this section, we describe offline goal-conditioned RL, the algorithms under consideration, and conclude the section with an overview of hyperparameter spaces and landscapes.

Offline GCRL. Our problem setting is a controlled Markov process without rewards $\mathcal{M} = (\mathcal{S}, \mathcal{A}, \mu, p)$ and an unlabeled dataset \mathcal{D} of trajectories (Park et al., 2025a). Here, \mathcal{S} denotes the state space, \mathcal{A} the action space, $\mu \in \Delta(\mathcal{S})$ the initial state distribution, where $\Delta(\mathcal{S})$ is the set of probability distributions in \mathcal{S} , and $p(s' | s, a) : \mathcal{S} \times \mathcal{A} \rightarrow \Delta(\mathcal{S})$ the transition dynamics. The dataset $\mathcal{D} = \{\tau^{(n)}\}_{n=1}^N$ consists of unlabeled trajectories $\tau^{(n)} = (s_0^{(n)}, a_0^{(n)}, s_1^{(n)}, \dots, s_{T_n}^{(n)})$. The goals are states $g \in \mathcal{S}$, and the objective of offline

GCRL is to learn a goal-conditioned policy $\pi(a \mid s, g) : \mathcal{S} \times \mathcal{S} \rightarrow \Delta(\mathcal{A})$ that reaches the goal state in as few time steps as possible. This objective is commonly formalized by maximizing the expected discounted return $\mathbb{E}_{\tau \sim p(\tau \mid g)} \left[\sum_{t=0}^T \gamma^t \delta_g(s_t) \right]$, where $T \in \mathbb{N}$ is the episode horizon, $\gamma \in (0, 1)$ is the discount factor, $p(\tau \mid g)$ is the trajectory distribution induced by μ , π , and p , and $\delta_g(s)$ denotes the indicator function for the goal state. Equivalently, this corresponds to optimizing a sparse reward with a clear goal, often written as $r(s, g) = \mathbb{1}[s = g]$.

Algorithms. We study two representative algorithms for bootstrapped TD learning and non-TD representation-learning. All methods operate on a fixed offline dataset and rely on self-supervised goal relabeling, where goals are sampled from states already present in the data. Following standard practice in offline GCRL benchmarks, we consider uniform and truncated geometric future-state sampling ($p_D^{\text{traj}}(g \mid s)$, $p_D^{\text{geom}}(g \mid s)$), as well as random-goal sampling $p_D^{\text{rand}}(g)$ and their mixtures; precise definitions and algorithm-specific usage are deferred to Section B.

Hierarchical Implicit Q-Learning (HIQL) (Park et al., 2023) instantiates the **bootstrapped TD-learning** paradigm. It learns a goal-conditioned value function $V(s, g)$ via expectile regression. Crucially, it uses an action-free objective with a bootstrapped target $y = r + \gamma V(s', g)$.

$$\mathcal{L}_{\text{HIQL}}(\theta) = \mathbb{E}_{(s, s', g) \sim \mathcal{D}} \left[L_2^\tau \left((r + \gamma V_{\bar{\psi}}(s', g)) - V_\theta(s, g) \right) \right], \quad (1)$$

where $L_2^\tau(u) = |\tau - \mathbb{1}(u < 0)|u^2$ is the expectile loss. Reliance on $V(s', g)$ means that updates are structurally coupled across the state space: changing the value estimate at s' immediately affects the target for s . Afterward, HIQL extracts a hierarchical policy from this value function.

Quasimetric RL (QRL) (Wang et al., 2023) instantiates the **representation learning** paradigm. Instead of bootstrapping reward expectations, it learns a latent quasimetric $d_\phi(s, g)$ using a specialized architecture (e.g., Interaction Quasimetric Embeddings) that *structurally guarantees* the triangle inequality. Consequently, rather than minimizing a Bellman error, QRL optimizes a dual objective that maximizes global distances subject to local transition constraints:

$$\max_{\phi} \mathbb{E}_{s, g \sim \mathcal{D}} [d_\phi(s, g)] \quad \text{s.t.} \quad \mathbb{E}_{(s, s') \sim \mathcal{D}} [(d_\phi(s, s') - 1)^2] \leq \varepsilon. \quad (2)$$

By organizing the latent space to satisfy these geometric constraints globally, QRL avoids the recursive target-dependency and error propagation characteristic of bootstrapped TD updates.

Hyperparameter landscapes in RL. Let Λ be a bounded hyperparameter space and let $f_t : \Lambda \rightarrow \mathbb{R}$ map a configuration $\lambda \in \Lambda$ to an evaluation metric (e.g., success rate) in the

training phase t . The induced response surface of f_t over Λ is the *hyperparameter landscape* at phase t ; variation of f_t across t captures training-time non-stationarity in what configurations are near-optimal. In Section 3, we operationalize landscapes using a phased data-collection pipeline and landscape analysis adapted from Mohan et al. (2023). Methodologically, our diagnostics follow the landscape-analysis tradition in algorithm configuration and AutoML: we quantify geometry via near-optimal mass and drift-style measures and identify influential knobs via variance attribution (fANOVA) (Pitzer and Affenzeller, 2012; Malan, 2021; Pushak and Hoos, 2020; 2022; Hutter et al., 2014; Sass et al., 2022).

3. Analysis Protocol and Experimental Setup

We study how offline GCRL objectives induce phase-dependent hyperparameter response functions under controlled dataset regimes, and we summarize these responses with complementary diagnostics that separate *which* hyperparameters matter from *how* optimization geometry evolves.

Phased training protocol. We adopt the phased pipeline of Mohan et al. (2023) to obtain phase-indexed response functions. A *phase* is a contiguous training segment that ends at the boundary $t_{\text{ls}}(i)$. At each boundary, we evaluate all configurations and start the next phase from a shared reference checkpoint (the checkpoint selected in the previous phase). This synchronization ensures that within-phase differences arise from hyperparameters and stochasticity rather than divergent training histories, making $f_t(\lambda)$ directly comparable across phases on the same configuration set C . Unlike Mohan et al. (2023), we evaluate at the respective phase boundary (rather than always at t_{final}), since it both increased compute and degraded performance in our setting (Table 9). We report a comparison in Table 9. More details on the training protocol are provided in Section D.

Evaluation metrics and checkpoint selection. We evaluate configurations using two complementary metrics: *success ratio* (binary task completion) and *goal-distance return* (a continuous progress proxy). We use success ratio as the *selection objective* for phase checkpointing to ensure task-competent agents. However, because binary metrics saturate and obscure the landscape geometry near the optimum, we use the continuous proxy as our *geometry probe* for response surfaces. Formally, for an episode starting at s_0 with the goal g and ending at s_T , we define the distance return of the goal $R_{\text{dist}}(s_T, g)$ as follows:

$$R_{\text{dist}}(s_T, g) = 1 - \frac{\|s_T - g\|_2}{\|s_0 - g\|_2}, \quad (3)$$

where $\|\cdot\|_2$ denotes Euclidean distance. This metric ranges from $(-\infty, 1]$, where 1 corresponds to reaching the goal

$(s_T=g)$ and 0 corresponds to not making progress ($s_T=s_0$). Unlike raw distance, this normalizes for task difficulty; unlike success rate, it distinguishes between "almost reaching the goal" and "moving in the wrong direction" (negative values), preventing flat landscape plateaus.

Hyperparameter importances. To identify which hyperparameters drive performance variability, we compute fANOVA importances (Hutter et al., 2014) using DeepCAVE (Segel et al., 2025) on evaluation data gathered via Bayesian optimization (SMAC (Lindauer et al., 2022) with Hypersweeper (Eimer, 2024)). For each phase, algorithm, and dataset setting, fANOVA returns an importance vector over tuned hyperparameters. We report phase-to-phase cosine distance; values near 0 indicate similar importance profiles, values near 1 indicate strong reordering.

Hyperparameter landscapes: geometry and transferability. Importances capture variance attribution, but not tunability (broad plateaus vs. sharp ridges) (Probst et al., 2019) or whether early choices remain good later. We therefore analyze pairwise response landscapes for selected hyperparameter pairs. For visualization only, we fit Independent Gaussian Process Regressors (IGPR) (Mohan et al., 2023). All metrics below use raw evaluations.

We summarize landscape geometry with three metrics: (i) **ε -optimality mass** ρ_ε , the fraction of evaluated configurations that achieve at least an ε fraction of the best observed performance at the given timestep:

$$\rho_\varepsilon = \frac{1}{|C|} \left| \left\{ \lambda \in C : f(\lambda) \geq \varepsilon \max_{\lambda' \in C} f(\lambda') \right\} \right|. \quad (4)$$

(ii) **phase-to-phase drift** $\Delta(t, t+1)$, the mean absolute change in configuration performance optimality between consecutive phases:

$$\Delta(t, t+1) = \frac{1}{|C|} \sum_{\lambda \in C} \left| \frac{f_{t+1}(\lambda)}{\max_{\lambda' \in C} f_{t+1}(\lambda')} - \frac{f_t(\lambda)}{\max_{\lambda' \in C} f_t(\lambda')} \right|. \quad (5)$$

(iii) **early-selection regret** $r_{t \rightarrow t'}(\lambda)$, the cost of committing to a configuration chosen in phase t when evaluated in a later phase $t' > t$:

$$r_{t'}(\lambda) = 1 - \frac{f_{t'}(\lambda)}{\max_{\lambda' \in C} f_{t'}(\lambda')}. \quad (6)$$

We average $r_{t'}(\lambda)$ over future phases $t' \in \{t+1, \dots, P\}$ to quantify transferability.

Mixed datasets and controlled non-stationarity. We vary data quality by mixing expert (*navigate*) and exploratory (*explore*) trajectories with an adjustable ratio.

Constant mixtures yield a stationary training distribution at a fixed quality level. To introduce controlled non-stationarity while remaining offline, we also use a *scheduled* regime that improves mixture quality across phases: 100% \rightarrow 80% \rightarrow 40% \rightarrow 0% explore. This intervention targets non-stationarity in *trajectory quality* (later data is more goal-directed) while keeping the interaction budget fixed. However, unlike online learning, our schedule does not change state coverage, helping separate the effect of trajectory quality on landscape robustness, drift, and regret.

Gradient interference diagnostics. Landscape metrics quantify robustness, drift, and transferability, but do not explain why some objectives yield tighter optima and stronger phase sensitivity. We therefore measure *inter-goal gradient alignment*, a variant of the gradient interference metrics prevalent in multitask learning (Yu et al., 2020), in the critic update: whether gradients induced by different goal relabelings reinforce or conflict.

Let θ denote the critic parameters (we report the critic trunk). For a minibatch $B = \{(s_i, a_i, s'_i)\}_{i=1}^n$ and relabeled goal g , let $\mathcal{L}(\theta; B, g)$ be the algorithm-specific critic loss (HIQL: TD/expectile regression; QRL: quasimetric objective with triangle-inequality regularization). Define

$$\mathbf{g}(g) = \nabla_\theta \mathcal{L}(\theta; B, g), \quad \tilde{\mathbf{g}}(g) = \frac{\mathbf{g}(g)}{\|\mathbf{g}(g)\|_2}. \quad (7)$$

For a set of relabeled goals $G(B)$ (sampled from the same relabeling distribution as training), we compute

$$\kappa(g, g') = \tilde{\mathbf{g}}(g)^\top \tilde{\mathbf{g}}(g'), \quad g \neq g'. \quad (8)$$

Negative $\kappa(g, g')$ indicates destructive interference. The concentration near 1 indicates highly similar update directions (which can also reflect weak goal dependence), so we interpret alignment together with geometry and performance. We summarize the distribution $\{\kappa(g, g')\}$ using the empirical CDF. Our hypothesis is that TD bootstrapping increases negative-tail mass and dispersion, consistent with tighter optima and stronger phase sensitivity in HIQL.

Implementation details. We log gradient diagnostics ten times throughout each phase using the same configuration set C as landscape evaluation, enabling phase-aligned comparisons between geometry, fANOVA stability, and gradient interference.

4. Experiments

We evaluate hyperparameter sensitivity in offline GCRL along two axes: (i) which hyperparameters explain performance variability (fANOVA), and (ii) how optimization geometry and transferability evolve across phases (landscape metrics in Equations (4) to (6)). Unless stated

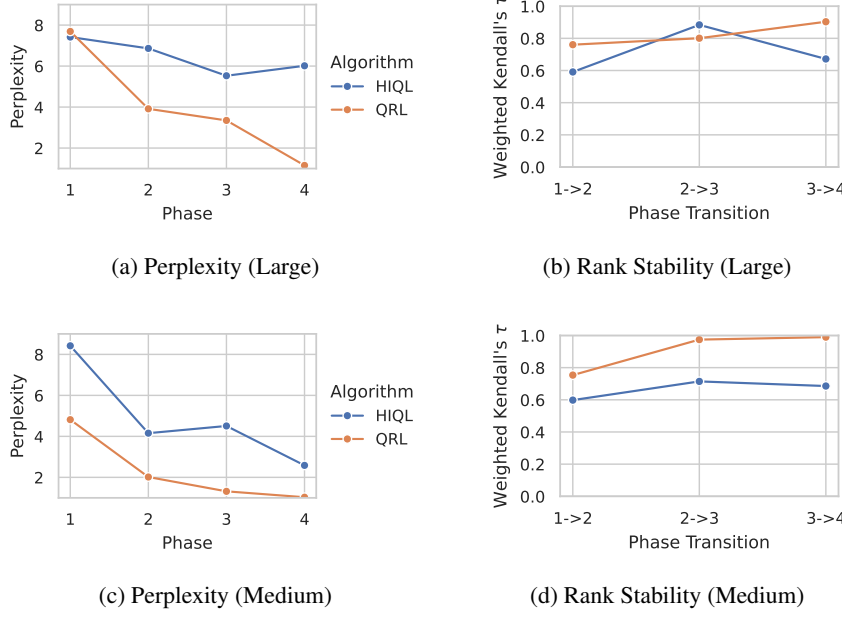


Figure 2. Phase-wise concentration and stability of FANOVA importances. We compare hyperparameter influence across scheduled data quality phases. **Left Column (a, c):** Perplexity of the normalized importance distribution; lower values indicate importance concentrates on fewer hyperparameters. **Right Column (b, d):** Importance-weighted Kendall’s τ between consecutive phases; higher values indicate a more stable ordering of influential hyperparameters. Results are shown for antmaze-large-v0 (**top**) and antmaze-medium-v0 (**bottom**).

otherwise, all reported numbers aggregate over 5 random seeds. For each (algorithm, phase, dataset regime), we evaluate 128 hyperparameter configurations, sampled using a scrambled Sobol sampling strategy (Sobol, 1967; Joe and Kuo, 2008). Each configuration is evaluated on 6 goals with 10 episodes per goal, and we report the performance as the interquartile mean (IQM) across seeds (Agarwal et al., 2021). For landscape visualizations, we use a subset of 64 configurations for the selected hyperparameter pairs (see Section 4.2). We evaluate hyperparameter importances on antmaze-large-v0 and antmaze-medium-v0. For hyperparameter landscape evaluation we add pointmaze-medium-v0, humanoidmaze-medium-v0 and antmaze-teleport-v0, unless specified otherwise.

4.1. Hyperparameter Importances

For importance, the phase-dependent response $f_t(\lambda)$ is the *success ratio*, measured on 6 evaluation goals and 10 episodes per goal. We study three dataset regimes: two stationary mixtures (0% explore and 90% explore), and a scheduled regime 100% \rightarrow 80% \rightarrow 40% \rightarrow 0% explore that mimics improving trajectory quality over training. All regimes are evaluated using 128 configurations with 5 random seeds each.

Comparability across objectives and hyperparameter spaces. HIQL and QRL expose different tunable hyperparameters (e.g., HIQL includes target-network update τ and hierarchy-specific knobs, while QRL includes quasimetric-regularization weights and related objective parameters). We therefore do not compare *per-hyperparameter* effects

across algorithms. Instead, for each algorithm, we analyze its own tuning space using a shared analysis protocol and identical compute budget, and we compare *space-level properties* across objectives: (i) how concentrated the importance distribution is (few knobs dominate vs. many matter), (ii) how stable importances are across phases, and (iii) how the response geometry behaves (near-optimal mass, drift, regret, and mobility). When a knob is shared (e.g. learning rate and discount factor), we also include matched 2D slices in the common (λ, γ) plane to support direct qualitative comparisons.

Representation learning yields stable, learning-rate-dominated importances. QRL exhibits largely stable importance profiles across phases and dataset regimes, typically dominated by the learning rate (Figure 2). The main exception is early training: in Phase 1, multiple hyperparameters contribute non-trivially before the learning rate dominates in later phases. This suggests that QRL’s quasimetric objective (distance-to-goal) is initially more brittle, and weak goal coverage and limited training can make multiple design choices matter simultaneously.

Bootstrapped TD learning is more data-sensitive. HIQL shows more distributed importance and stronger dependence on dataset quality than QRL (Figure 6 and Appendix Section E). In stationary settings, HIQL importances are comparatively stable across phases, whereas scheduling induces larger shifts, indicating that the identity of influential hyperparameters changes as data quality improves.

Dataset regime	Algorithm	Phase Transition		
		1→2	2→3	3→4
0%	HIQL	0.165	0.0275	0.031
	QRL	0.814	0.000	0.000
Scheduled	HIQL	0.405	0.427	0.360
	QRL	0.595	0.0295	0.023

Table 1. Phase-to-phase change in hyperparameter importance profiles. Entries report cosine distance $d = 1 - \cos(\mathbf{v}_t, \mathbf{v}_{t+1})$ between phase-wise fANOVA importance vectors (rounded to three decimals). Scheduled data quality corresponds to 100% → 80% → 40% → 0% exploration noise ratio. We average over antmaze-medium-v0 and antmaze-large-v0.

Quantifying stability across phases. We summarize importance stability using the cosine distance between phase-wise fANOVA vectors (Table 1). HIQL exhibits the largest phase-to-phase changes across dataset regimes. For QRL, most of the observed change concentrates in the transition from Phase 1 to Phase 2, consistent with early-learning transients.

Takeaway (Importances). Under stationary data, QRL concentrates sensitivity in a small subset of hyperparameters, dominated by the learning rate after early training. HIQL exhibits more distributed and data-quality-dependent importances, suggesting that bootstrapped TD learning requires tuning a broader set of hyperparameters and that the relevant knobs can shift as data quality changes.

Scheduled data quality importances. Figure 2 summarizes the phase-wise importance under scheduled data quality. Importances alone do not reveal whether these shifts correspond to significant changes in optimization geometry. We therefore turn to landscape-based diagnostics that directly quantify robustness, drift, and transferability.

4.2. Hyperparameter Landscapes

We analyze pairwise response landscapes for learning rate and discount factor, identified as dominant hyperparameters in Appendix Section E. We evaluated 64 configurations per landscape (5 seeds) across the qualities of the data set ($\{0, 40, 80, 100\}\%$ exploration noise). Unless otherwise specified, the same goal-sampling mechanisms are used across all algorithms.

ε -optimality mass. We quantify robustness via ρ_ε (Equation (4)), the fraction of near-optimal configurations. Table 2 compares the aggregated ε -optimality across phases in scheduled versus constant regimes. Both regimes exhibit substantial near-optimal mass across phases, indicating

broadly benign landscapes. In the final phase, scheduling increases ρ_ε and mean performance, consistent with expert data stabilizing the objective. HIQL shows weaker gains at $\varepsilon=0.9$ vs. $\varepsilon=0.8$, suggesting its peak region is less stable than the bulk near-optimal area. Across algorithms, a large fraction of configurations remain near-optimal, especially once expert data is present.

Non-stationarity: regret and drift. To test the validity of early tuning, we measure early-selection regret (Equation (6)) and phase-to-phase drift (Equation (5)). Most landscape reorganization happens early: after the first phase transition, both drift and early-selection regret drop sharply. Scheduling data quality prolongs this early instability, but once modest expert content is present, landscapes become largely stationary and early configuration choices transfer reliably.

Non-stationarity: visualization. While metrics quantify sensitivity to changes in hyperparameter configurations, they abstract away *where* the optima move and whether interactions create narrow ridges. We therefore visualize 2D response surfaces (via IGPR) to inspect (i) optimal region shifts and (ii) interaction structures. Figure 1 shows near-optimal landscapes under scheduled (top) and fixed (bottom) regimes. Under schedules, QRL exhibits mild interactions and broad optimal regions once expert data appears. HIQL, on the other hand, shows tighter optima and stronger interactions, indicating higher sensitivity to the schedule. Across dataset qualities, QRL remains qualitatively stable, with near-optimal regions persisting as long as the learning rate is not extreme. HIQL instead exhibits a clear regime shift between low- and high-noise datasets, characterized by smaller near-optimal regions and more pronounced interactions in the high-noise regime.

Takeaway (Landscapes). In general, landscapes tend to have high numbers of near-optimal configurations. Most non-stationarity happens at the beginning of training, especially under scheduled dataset quality, when little expert data is present. Contrasting the two algorithms, HIQL shows tighter optima and stronger interactions under constant and scheduled regimes, suggesting higher sensitivity to the data’s distribution and hyperparameters in general.

4.3. Gradient Alignment Analysis

The landscape results above reveal a consistent qualitative gap: HIQL exhibits tighter optima and stronger phase sensitivity than QRL under the same offline dataset regimes. This suggests that objective-level design choices can induce sensitivity to hyperparameter configurations even without exploration-driven non-stationarity. We therefore study

Setting	Algorithm	All Phases				Last Phase			
		$\rho_{0.9}$	$\rho_{0.8}$	Mean(f)	Max(f)	$\rho_{0.9}$	$\rho_{0.8}$	Mean(f)	Max(f)
Scheduled	HIQL	0.12 \pm 0.10	0.29 \pm 0.20	0.30 \pm 0.17	0.80	0.21 \pm 0.10	0.52 \pm 0.08	0.44 \pm 0.19	0.84
	QRL	0.35 \pm 0.25	0.54 \pm 0.28	0.40 \pm 0.22	0.80	0.48 \pm 0.29	0.80 \pm 0.03	0.56 \pm 0.14	0.80
Constant	HIQL	0.13 \pm 0.10	0.30 \pm 0.19	0.33 \pm 0.15	0.92	0.20 \pm 0.10	0.42 \pm 0.18	0.40 \pm 0.16	0.92
	QRL	0.33 \pm 0.23	0.53 \pm 0.26	0.40 \pm 0.20	0.86	0.45 \pm 0.19	0.66 \pm 0.15	0.45 \pm 0.21	0.84

Table 2. Near-optimal mass and absolute performance of landscapes under scheduled vs. constant data quality. For each setting and algorithm, we evaluate a fixed set of configurations C in each phase. 0.9 **Ratio** (resp. 0.8 **Ratio**) reports the ε -optimality mass ρ_ε with $\varepsilon = 0.9$ (resp. 0.8), computed *per phase*. **Mean** is the average of $f(\lambda)$ over $\lambda \in C$ (per phase), and **Max** is $\max_{\lambda \in C} f(\lambda)$ (per phase). All measures are averaged over antmaze-medium-v0 and antmaze-large-v0. The **All Phases** block reports the mean \pm std of these per-phase quantities across phases; the **Last Phase** block reports the corresponding quantities for Phase 4 only. Example: a 0.9 **Ratio** of 0.20 means 20% of configurations achieve at least 90% of the best configuration in that phase.

Setting	Algorithm	Early Selection Regret		Across-Phase Change	
		Pick Phase 1	Pick Phase 2	Per Algorithm	
Scheduled	HIQL	0.25 \pm 0.03	0.18 \pm 0.17	0.22 \pm 0.16	
	QRL	0.42 \pm 0.13	0.04 \pm 0.01	0.17 \pm 0.11	
Constant	HIQL	0.14 \pm 0.11	0.09 \pm 0.06	0.16 \pm 0.11	
	QRL	0.11 \pm 0.07	0.06 \pm 0.02	0.14 \pm 0.12	

Table 3. Early-selection regret and algorithm-wise across-phase change under scheduled and constant-noise datasets. Early-selection regret measures sensitivity to when a configuration is selected, while across-phase change measures algorithm-wise instability across training phases. For across-phase change, we calculate how much a configuration’s performance changes on average over all phases, while normalizing each phase with the maximum performance. Values report mean \pm standard deviation. The data was gathered on antmaze-large-v0 and antmaze-medium-v0.

Setting	Transition	Change	
		1 \rightarrow 2	0.36 \pm 0.09
Scheduled	2 \rightarrow 3	0.15 \pm 0.02	
	3 \rightarrow 4	0.08 \pm 0.03	
	1 \rightarrow 2	0.29 \pm 0.08	
Constant	2 \rightarrow 3	0.08 \pm 0.04	
	3 \rightarrow 4	0.07 \pm 0.04	

Table 4. Phase-to-phase change in per-phase normalized performance (goal distance return, scaled by the maximal performance in that phase) under scheduled and constant-noise datasets. The data was gathered on antmaze-large-v0 and antmaze-medium-v0.

gradient interference as a diagnostic: whether objectives that rely on bootstrapped targets are *associated* with more frequent conflicting goal-conditioned critic updates, and whether this association tracks the same regimes where landscapes appear sharper and less transferable.

What gradients we measure (and what we do not). Our diagnostic is computed *only* on critic/value gradients. Concretely, for each algorithm, we log gradients with respect to the shared critic parameters (critic trunk) under the algorithm’s critic loss for a given goal relabeling. We compute gradients at fixed points *within* each phase (ten logging events per phase), using the same configuration set C as landscape evaluation to allow phase-aligned comparisons. For each logging event, we sample relabeled goals using the *same* goal relabeling distribution as training for that configuration (held fixed within the logging event), and compute gradients for multiple goals on the same minibatch. For QRL, we differentiate the implemented quasimetric critic loss (including the triangle-inequality regularization in its penalty form, as used in our training code); for HIQL, we differentiate the bootstrapped expectile regression loss used for value learning.

HIQL exhibits less complementing gradients. In Figure 3, the actor distributions are comparatively tight and centered near 0, whereas the critic distributions, especially for HIQL, exhibit much broader spread and heavier negative mass, suggesting that most cross-goal interference arises in value learning rather than in policy updates. On average, HIQL shows a heavier negative tail of similarities, indicating more destructive interference among gradients. It also shows a heavier positive tail, suggesting that gradients do not complement each other and may therefore lack goal-specific information. We observe that for HIQL, the standard deviation of the distribution correlates with the regret of the configuration (Pearson correlation of 0.43), indicating that tail heaviness is associated with lower performance in configurations. The most influential factor in predicting the width of QRL’s alignment distribution is the number of training steps we have taken (Pearson correlation of 0.21), indicating how close to convergence we are. Taking into account only small changes in this distribution across environments and configurations (Figure 3), this suggests that QRL’s gradient alignment is mostly independent of the configuration and environment.

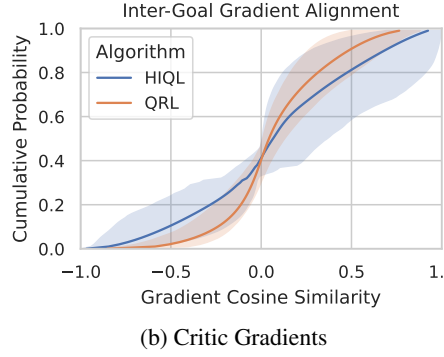
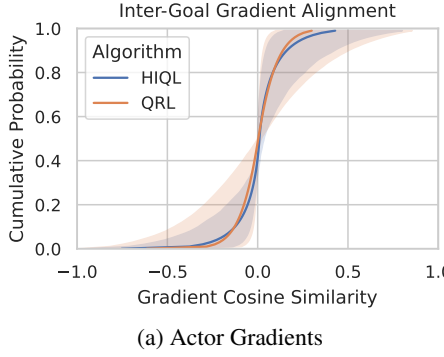


Figure 3. Inter-goal gradient alignment. Empirical CDF of cosine similarity $\kappa(g, g')$ between gradients induced by different goal relabelings. More negative similarities indicate stronger inter-goal interference. HIQL exhibits substantially more negative mass than QRL, especially in the critic updates, suggesting that bootstrapped targets being associated with sensitivity to the hyperparameters studied.

Why bootstrapping may amplify conflicts (interpretation). When different goals impose incompatible target constraints, their gradients can conflict, potentially shrinking the set of hyperparameters that allow stable learning. This interpretation is consistent with our fANOVA and contour-plot findings: HIQL shows the strongest phase-to-phase importance shifts under scheduled data quality (Figure 2) and the tightest high-performance regions on response surfaces (Figure 1). In contrast, QRL exhibits a substantially weaker negative tail, with similarities concentrating closer to 0, aligning with the broader near-optimal regions we observe once early transients pass.

Takeaway (Gradients). Inter-goal gradient interference, captured by the heaviness of the negative tail of the cosine similarity distribution, is a diagnostic that *covaries* with low performance. For HIQL (TD-Learning), interference was found to be tied to hyperparameter configurations, while for QRL, this was not the case.

Controls, limitations, and residual confounders. Cosine similarity is a diagnostic criterion, not an optimality criterion: high alignment can reflect either coherent generalization or insufficient goal sensitivity. Our diagnostic focuses on critic/value gradients, isolating interference in value learning rather than interference arising from policy optimization. Moreover, HIQL and QRL differ in more than bootstrapping (e.g., objective, regularization, and update rules), so cross-algorithm comparisons alone do not establish causality. We therefore interpret gradient alignment jointly with landscape geometry and absolute performance, treating it as a descriptive mechanism consistent with the observed patterns rather than a definitive explanation.

5. Conclusion

We analyzed hyperparameter sensitivity in offline GCRL with phase-resolved diagnostics that separate *which* hyperparameters matter from *how* their effects evolve over training. Overall, we observed more benign hyperparameter inter-

actions during training than previously reported in online RL (Mohan et al., 2023). However, in controlled mixtures of exploratory and expert data, we observed a clear split at the objective level. The non-bootstrapped quasimetric objective (QRL) induces smooth response landscapes with broad near-optimal regions once modest expert content is present. In contrast, the bootstrapped TD method (HIQL) exhibits sharper optima and substantial phase-to-phase drift, most prominently under scheduled shifts in data quality that introduce training-time non-stationarity. This demonstrates that hyperparameter brittleness can persist even when exploration-induced distribution shift is removed and that the resulting instability is strongly phase dependent. Our evidence points to *inter-goal update interference* as a plausible driver. We hypothesize that bootstrapped targets in HIQL are consistent with systematically more conflicting goal-conditioned updates, reflected in a heavier negative tail of gradient cosine similarity, and this effect co-occurs with heightened sensitivity to target-shaping hyperparameters such as learning rate and discount factor. It suggests that the objective structure does not merely change average performance: it changes the geometry and transferability of good hyperparameter regions across phases. Practically, these results suggest that, in offline GCRL with any nontrivial expert fraction, non-TD objectives may reduce the need for complex phase-specific hyperparameter optimization schedules, whereas TD-style methods may require either retuning or explicit stabilization.

Limitations and scope. Our conclusions are based on two representative objectives, and we use offline GCRL precisely because it improves interpretability by removing the exploration-induced distribution shift. Even under fixed environment dynamics, scheduled changes in data quality can induce drifting optima in hyperparameter configurations in TD-style methods, consistent with destructive inter-goal interference. An important direction for future work is to design objectives or update rules that preserve the sample-efficiency benefits of bootstrapping while mitigating cross-goal conflicts that undermine robustness.

6. Impact Statement

This work contributes to a clearer understanding of when and under what conditions hyperparameter sensitivity arises in offline goal-conditioned RL. Practically, these findings may reduce trial-and-error tuning (and associated compute cost) by highlighting sensitivity to training schedules and data-quality changes, which can improve reproducibility. A potential downstream effect is lowering the barrier to applying offline RL in practice, including in higher-stakes domains; however, our results are diagnostic and do not constitute a deployment-ready method. Safe real-world use would still require domain-specific validation, monitoring, and attention to issues such as bias, fairness, and misuse.

References

Proceedings of the 39th International Conference on Advances in Neural Information Processing Systems (NeurIPS'25), 2025. Curran Associates.

J. Adkins, M. Bowling, and A. White. A method for evaluating hyperparameter sensitivity in reinforcement learning. In *Proceedings of the 38th International Conference on Advances in Neural Information Processing Systems (NeurIPS'24)*. Curran Associates, 2024.

R. Agarwal, D. Schuurmans, and M. Norouzi. An optimistic perspective on offline reinforcement learning. In *Proceedings of the 37th International Conference on Machine Learning, ICML*, volume 119 of *Proceedings of Machine Learning Research*, pages 104–114. PMLR, 2020.

R. Agarwal, M. Schwarzer, P. Samuel Castro, A. C. Courville, and M. G. Bellemare. Deep reinforcement learning at the edge of the statistical precipice. In Ranzato et al. (2021).

M. Andrychowicz, F. Wolski, A. Ray, J. Schneider, R. Fong, P. Welinder, B. McGrew, J. Tobin, P. Abbeel, and W. Zaremba. Hindsight experience replay. In *Proceedings of the 32nd International Conference on Advances in Neural Information Processing Systems (NeurIPS'17)*, 2017.

M. Andrychowicz, A. Raichuk, P. Stańczyk, M. Orsini, S. Girgin, R. Marinier, L. Hussenot, M. Geist, O. Pietquin, M. Michalski, S. Gelly, and O. Bachem. What matters for on-policy deep actor-critic methods? a large-scale study. In *The Ninth International Conference on Learning Representations (ICLR'21)*. ICLR, 2021. Published online: [iclr.cc](https://openreview.net/forum?id=v1UK2h1Nvw).

J. Becktepe, J. Dierkes, C. Benjamins, A. Mohan, D. Salinas, R. Rajan, F. Hutter, H. Hoos, M. Lindauer, and T. Eimer. Arlbench: Flexible and efficient benchmarking for hyperparameter optimization in reinforcement learning. In *17th European Workshop on Reinforcement Learning (EWRL)*, 2024.

J. Dierkes, E. Cramer, H. Hoos, and S. Trimpe. Combining automated optimisation of hyperparameters and reward shape. *Reinforcement Learning Journal*, 2024.

T. Eimer. Hypersweeper, 2024. URL <https://github.com/automl/hypersweeper>.

T. Eimer, A. Biedenkapp, F. Hutter, and M. Lindauer. Self-paced context evaluation for contextual reinforcement learning. In M. Meila and T. Zhang, editors, *Proceedings of the 38th International Conference on Machine Learning (ICML'21)*, volume 139 of *Proceedings of Machine Learning Research*, pages 2948–2958. PMLR, 2021.

T. Eimer, M. Lindauer, and R. Raileanu. Hyperparameters in reinforcement learning and how to tune them. In Krause et al. (2023).

L. Engstrom, A. Ilyas, S. Santurkar, D. Tsipras, F. Janoos, L. Rudolph, and A. Madry. Implementation matters in deep RL: A case study on PPO and TRPO. In *The Eighth International Conference on Learning Representations (ICLR'20)*. ICLR, 2020. Published online: [iclr.cc](https://openreview.net/forum?id=v1UK2h1Nvw).

J. Farebrother and P. Castro. CALE: Continuous arcade learning environment. In *The Thirty-eight Conference on Neural Information Processing Systems Datasets and Benchmarks Track*, 2024. URL <https://openreview.net/forum?id=v1UK2h1Nvw>.

D. Foster and P. Dayan. Structure in the space of value functions. *Machine Learning*, 2002.

S. Fujimoto and S. Gu. A minimalist approach to offline reinforcement learning. In Ranzato et al. (2021).

S. Fujimoto, D. Meger, and D. Precup. Off-policy deep reinforcement learning without exploration. In K. Chaudhuri and R. Salakhutdinov, editors, *Proceedings of the 36th International Conference on Machine Learning (ICML'19)*, volume 97. Proceedings of Machine Learning Research, 2019.

D. Ghosh, C. Bhatteja, and S. Levine. Reinforcement learning from passive data via latent intentions. In Krause et al. (2023).

P. Henderson, R. Islam, P. Bachman, J. Pineau, D. Precup, and D. Meger. Deep reinforcement learning that matters. In S. McIlraith and K. Weinberger, editors, *Proceedings of the Thirty-Second Conference on Artificial Intelligence (AAAI'18)*. AAAI Press, 2018.

F. Hutter, H. Hoos, and K. Leyton-Brown. An efficient approach for assessing hyperparameter importance. In

E. Xing and T. Jebara, editors, *Proceedings of the 31th International Conference on Machine Learning, (ICML'14)*, pages 754–762. Omnipress, 2014.

F. Hutter, L. Kotthoff, and J. Vanschoren, editors. *Automated Machine Learning: Methods, Systems, Challenges*. Springer, 2019. Available for free at <http://automl.org/book>.

Proceedings of the International Conference on Learning Representations (ICLR'22), 2022. ICLR. Published online: iclr.cc.

Proceedings of the International Conference on Learning Representations (ICLR'25), 2025. ICLR. Published online: iclr.cc.

M. Jaderberg, V. Dalibard, S. Osindero, W. Czarnecki, J. Donahue, A. Razavi, O. Vinyals, T. Green, I. Dunning, K. Simonyan, C. Fernando, and K. Kavukcuoglu. Population based training of neural networks. *arXiv:1711.09846 [cs.LG]*, 2017.

S. Joe and F. Kuo. Constructing sobol sequences with better two-dimensional projections. *SIAM J. Sci. Comput.*, 2008.

I. Kostrikov, A. Nair, and S. Levine. Offline reinforcement learning with implicit q-learning. In *The Tenth International Conference on Learning Representations (ICLR'22)* ICL (2022). Published online: iclr.cc.

A. Krause, E. Brunskill, K. Cho, B. Engelhardt, S. Sabato, and J. Scarlett, editors. *Proceedings of the 40th International Conference on Machine Learning (ICML'23)*, volume 202 of *Proceedings of Machine Learning Research*, 2023. PMLR.

A. Kumar, J. Fu, M. Soh, G. Tucker, and S. Levine. Stabilizing off-policy q-learning via bootstrapping error reduction. In H. Wallach, H. Larochelle, A. Beygelzimer, F. d'Alche Buc, E. Fox, and R. Garnett, editors, *Proceedings of the 33rd International Conference on Advances in Neural Information Processing Systems (NeurIPS'19)*. Curran Associates, 2019.

A. Kumar, A. Zhou, G. Tucker, and S. Levine. Conservative q-learning for offline reinforcement learning. In Larochelle et al. (2020).

H. Larochelle, M. Ranzato, R. Hadsell, M.-F. Balcan, and H. Lin, editors. *Proceedings of the 34th International Conference on Advances in Neural Information Processing Systems (NeurIPS'20)*, 2020. Curran Associates.

S. Levine, A. Kumar, G. Tucker, and J. Fu. Offline reinforcement learning: Tutorial, review, and perspectives on open problems. *CoRR*, abs/2005.01643, 2020. URL <https://arxiv.org/abs/2005.01643>.

M. Lindauer, K. Eggensperger, M. Feurer, A. Biedenkapp, D. Deng, C. Benjamins, T. Ruhkopf, R. Sass, and F. Hutter. SMAC3: A versatile bayesian optimization package for Hyperparameter Optimization. *Journal of Machine Learning Research*, 23(54):1–9, 2022.

Y. Ma, J. Yan, D. Jayaraman, and O. Bastani. Offline goal-conditioned reinforcement learning via f-advantage regression. In S. Koyejo, S. Mohamed, A. Agarwal, D. Belgrave, K. Cho, and A. Oh, editors, *Proceedings of the 36th International Conference on Advances in Neural Information Processing Systems (NeurIPS'22)*. Curran Associates, 2022.

K. Malan. A survey of advances in landscape analysis for optimisation. *Algorithms*, 2021.

Y. Mao, H. Zhang, C. Chen, Y. Xu, and X. Ji. Supported value regularization for offline reinforcement learning. In Oh et al. (2023).

A. Mohan, C. Benjamins, K. Wienecke, A. Dockhorn, and M. Lindauer. Autorl hyperparameter landscapes. In A. Faust, C. White, F. Hutter, R. Garnett, and J. Gardner, editors, *Proceedings of the Second International Conference on Automated Machine Learning*. Proceedings of Machine Learning Research, 2023.

A. Mohan, A. Zhang, and M. Lindauer. Structure in deep reinforcement learning: A survey and open problems. *Journal of Artificial Intelligence Research*, 79, 2024.

A. Mohan, T. Eimer, C. Benjamins, M. Lindauer, and A. Biedenkapp. Mighty: A comprehensive tool for studying generalization, meta-RL and autoRL. In *Eighteenth European Workshop on Reinforcement Learning*, 2025.

V. Myers, C. Ji, and B. Eysenbach. Horizon generalization in reinforcement learning. In *The Thirteenth International Conference on Learning Representations (ICLR'25)* ICL (2025). Published online: iclr.cc.

V. Myers, B. Chunyuan Zheng, B. Eysenbach, and S. Levine. Offline goal-conditioned reinforcement learning with quasimetric representations. In *Proceedings of the 38th International Conference on Advances in Neural Information Processing Systems (NeurIPS'25)* neu (2025).

A. Nair, A. Gupta, M. Dalal, and S. Levine. Awac: Accelerating online reinforcement learning with offline datasets. *arXiv preprint arXiv:2006.09359*, 2020.

J. Obando-Ceron, J. Araújo, A. Courville, and P. Castro. On the consistency of hyper-parameter selection in value-based deep reinforcement learning. *RLJ*, 3:1037–1059, 2024.

A. Oh, T. Naumann, A. Globerson, K. Saenko, M. Hardt, and S. Levine, editors. *Proceedings of the 37th International Conference on Advances in Neural Information Processing Systems (NeurIPS'23)*, 2023. Curran Associates.

S. Park, D. Ghosh, B. Eysenbach, and S. Levine. Hiql: Offline goal-conditioned rl with latent states as actions. In Oh et al. (2023).

S. Park, K. Frans, B. Eysenbach, and S. Levine. Og-bench: Benchmarking offline goal-conditioned rl. In *The Thirteenth International Conference on Learning Representations (ICLR'25)* ICL (2025). Published online: iclr.cc.

S. Park, K. Frans, D. Mann, B. Eysenbach, A. Kumar, and S. Levine. Horizon reduction makes RL scalable. In *Proceedings of the 38th International Conference on Advances in Neural Information Processing Systems (NeurIPS'25)* neu (2025).

J. Parker-Holder, V. Nguyen, and S. J. Roberts. Provably efficient online Hyperparameter Optimization with population-based bandits. In Larochelle et al. (2020).

J. Parker-Holder, R. Rajan, X. Song, A. Biedenkapp, Y. Miao, T. Eimer, B. Zhang, V. Nguyen, R. Calandra, A. Faust, F. Hutter, and M. Lindauer. Automated reinforcement learning (AutoRL): A survey and open problems. *Journal of Artificial Intelligence Research (JAIR)*, 74:517–568, 2022.

X. Peng, A. Kumar, G. Zhang, and S. Levine. Advantage-weighted regression: Simple and scalable off-policy reinforcement learning. *arXiv preprint arXiv:1910.00177*, 2019.

E. Pitzer and M. Affenzeller. A comprehensive survey on fitness landscape analysis. *Recent Advances in Intelligent Engineering Systems*, 2012.

P. Probst, A. Boulesteix, and B. Bischl. Tunability: Importance of hyperparameters of machine learning algorithms. *Journal of Machine Learning Research*, 20(53):1–32, 2019.

Y. Pushak and H. Hoos. Golden parameter search: exploiting structure to quickly configure parameters in parallel. In J. Ceberio, editor, *Proceedings of the Genetic and Evolutionary Computation Conference (GECCO'20)*, pages 245–253. ACM Press, 2020.

Y. Pushak and H. Hoos. Automl loss landscapes. *ACM Transactions on Evolutionary Learning and Optimization*, 2(3):1–30, 2022.

M. Ranzato, A. Beygelzimer, K. Nguyen, P. Liang, J. Vaughan, and Y. Dauphin, editors. *Proceedings of the 35th International Conference on Advances in Neural Information Processing Systems (NeurIPS'21)*, 2021. Curran Associates.

A. Saltelli, M. Ratto, T. Andres, F. Campolongo, J. Cariboni, D. Gatelli, M. Saisana, and S. Tarantola. *Global sensitivity analysis: the primer*. John Wiley & Sons, 2008.

R. Sass, E. Bergman, A. Biedenkapp, F. Hutter, and M. Lindauer. Deepcave: An interactive analysis tool for automated machine learning. In M. Mutny, I. Bogunovic, W. Neiswanger, S. Ermon, Y. Yue, and A. Krause, editors, *ICML Adaptive Experimental Design and Active Learning in the Real World (ReALML Workshop 2022)*, 2022.

T. Schaul, D. Horgan, K. Gregor, and D. Silver. Universal value function approximators. In F. Bach and D. Blei, editors, *Proceedings of the 32nd International Conference on Machine Learning (ICML'15)*, volume 37. Omnipress, 2015.

S. Segel, H. Graf, E. Bergman, K. Thieme, M. Wever, A. Tornede, F. Hutter, and M. Lindauer. Deepcave: A visualization and analysis tool for automated machine learning. *Journal of Machine Learning Research (MLOSS)*, 26(24):1–8, 2025.

I. Sobol. On the distribution of points in a cube and the approximate evaluation of integrals. *USSR Computational Mathematics and Mathematical Physics*, 7(4):86–112, 1967.

R. S. Sutton and A. G. Barto. *Reinforcement learning: An introduction*. Adaptive computation and machine learning. MIT Press, 2 edition, 2018.

D. Tarasov, A. Nikulin, D. Akimov, V. Kurenkov, and S. Kolesnikov. Corl: Research-oriented deep offline reinforcement learning library. In Oh et al. (2023).

J. Tsitsiklis and B. Van Roy. Analysis of temporal-difference learning with function approximation. 1996.

T. Wang, A. Torralba, P. Isola, and A. Zhang. Optimal goal-reaching reinforcement learning via quasimetric learning. In Krause et al. (2023).

R. Yang, Y. Lu, W. Li, H. Sun, M. Fang, Y. Du, X. Li, L. Han, and C. Zhang. Rethinking goal-conditioned supervised learning and its connection to offline rl. In *The Tenth International Conference on Learning Representations (ICLR'22)* ICL (2022). Published online: iclr.cc.

T. Yu, S. Kumar, A. Gupta, S. Levine, K. Hausman, and C. Finn. Gradient surgery for multi-task learning. In Larochelle et al. (2020).

B. Zhang, R. Rajan, L. Pineda, N. Lambert, A. Biedenkapp, K. Chua, F. Hutter, and R. Calandra. On the importance of Hyperparameter Optimization for model-based reinforcement learning. In A. Banerjee and K. Fukumizu, editors, *Proceedings of the 24th International Conference on Artificial Intelligence and Statistics (AISTATS'21)*, pages 4015–4023. Proceedings of Machine Learning Research, 2021.

B. Zheng, V. Myers, B. Eysenbach, and S. Levine. Multi-step quasimetric learning for scalable goal-conditioned reinforcement learning. *CoRR*, abs/2511.07730, 2025.

Appendix

Table of Contents

A	Related Work	13
B	Algorithmic Details	15
B.1	Self-Supervised Goal Relabeling	15
B.2	Hierarchical Implicit Q-Learning (HIQL)	15
B.3	Quasimetric RL (QRL)	16
C	Hyperparameters	16
D	Phased Training	16
D.1	Phase Splitting	17
E	fANOVA importance estimation details	18
E.1	Phase-wise fANOVA profiles under scheduled data quality	19
F	Hyperparameter Landscape Construction and Analysis	19
F.1	Phase selection	19
F.2	Hyperparameter spaces and configuration sampling	20
F.3	Landscape datasets and checkpoint resets	20
F.4	Landscape modeling and visualization	21
F.5	Reproducibility details	21
F.6	Phase Mobility Plots	22

A. Related Work

Our study connects three threads: (i) hyperparameter sensitivity and nonstationarity in RL, (ii) landscape-oriented analysis in AutoML, and (iii) offline goal-conditioned RL as a controlled setting for isolating objective-induced brittleness. We use the term *landscape* to refer to the *configuration-to-performance response surface* (hyperparameters \rightarrow return), not the weight-space loss landscape studied in deep learning. This distinction matters because our metrics quantify the geometry and transferability of *near-optimal hyperparameter regions* across training phases.

Hyperparameter sensitivity in deep RL. A recurring empirical finding is that deep RL is unusually sensitive to hyperparameter choices, leading to high variance between seeds and substantial tuning effort (Henderson et al., 2018; Parker-Holder et al., 2022; Farebrother and Castro, 2024). Large-scale studies show that performance variation is often dominated by a small subset of hyperparameters and that simple search methods can be competitive when budgets are sufficient (Eimer et al., 2023; Obando-Ceron et al., 2024). Other work emphasizes that architectural or algorithmic modifications that improve performance can also increase sensitivity, making robustness to hyperparameters a central objective rather than a byproduct (Adkins et al., 2024). Hyperparameter interactions have also been documented, including cases where agent and reward-shaping parameters are jointly dependent, which can create narrow viable regions even when individual knobs appear benign (Dierkes et al., 2024). Related reproducibility work shows that apparent sensitivity is often amplified by implementation details and evaluation protocol choices, motivating standardized pipelines and robust aggregate metrics (Engstrom et al., 2020; Agarwal et al., 2021; Mohan et al., 2025).

Training-time nonstationarity and dynamic tuning. Beyond cross-task brittleness, several works observe that well-performing hyperparameter configuration can change over the course of learning due to evolving data distributions and targets (Parker-Holder et al., 2022). Population-Based Training (PBT) explicitly exploits this by adapting hyperparameters online and often discovers schedules that outperform static configurations (Jaderberg et al., 2017). Closer to our protocol, phased evaluation pipelines reveal phase-dependent optima and measurable landscape drift in online RL, suggesting that nonstationarity can be substantial even within a fixed algorithm-environment pair (Mohan et al., 2023). Related evidence also appears in model-based RL, where automatic HPO can outperform expert tuning and where adaptivity is beneficial when learning dynamics change over time (Zhang et al., 2021). These results motivate our use of phase-resolved diagnostics, but they also highlight a limitation of the online setting: exploration and bootstrapped targets co-evolve, making it difficult to attribute brittleness to a specific mechanism. Beyond exploration-driven shifts, bootstrapped value learning induces *target nonstationarity*, and classic results identify the combination of function approximation, bootstrapping, and off-policy learning (the “deadly triad”) as a source of instability and brittleness (Tsitsiklis and Roy, 1996; Sutton and Barto, 2018). This motivates our focus on offline GCRL: by fixing the dataset, we can study phase-dependent response surfaces while reducing the confounding effects of online data collection.

Fitness landscapes and response-surface analysis. Landscape analysis is a standard lens in algorithm configuration and AutoML (Hutter et al., 2019) for studying structure in the *hyperparameter response surface* (configuration \rightarrow performance), including robustness, modality, and the geometry of near-optimal regions (Pitzer and Affenzeller, 2012; Malan, 2021). This differs from weight-space loss landscape analyses in deep networks, which study geometric properties of the training objective in parameter space. In combinatorial optimization and machine learning, low-dimensional response slices often exhibit regularities (e.g., unimodality in certain projections) that can be exploited algorithmically (Pushak and Hoos, 2020; 2022). In RL specifically, surface response studies during training progress provide evidence that optimal drift and that interaction strength can vary between phases, motivating phase-aware analysis and transfer diagnostics (Mohan et al., 2023). Our landscape metrics (ε -optimality mass, drift, and early-selection regret) follow this tradition, but we apply them in offline GCRL to decouple objective-induced effects from exploration-induced nonstationarity.

Offline RL and offline goal-conditioned RL as a controlled testbed. Offline RL fixes the distribution of the dataset and removes the exploration-induced distribution shift, offering a natural test bed to isolate algorithmic instabilities that persist without online data collection (Agarwal et al., 2020; Levine et al., 2020). However, offline RL is still subject to distribution shift between learned policy and dataset (OOD actions), and bootstrapping can amplify errors (Mao et al., 2023). Prominent offline RL approaches include behavior-regularized or constrained methods (Fujimoto et al., 2019; Kumar et al., 2019), conservative value learning (Kumar et al., 2020), and actor-critic variants that regularize toward behavior (Nair et al., 2020; Fujimoto and Gu, 2021), as well as implicit value-based methods such as IQ-L and its variants (Kostrikov et al., 2022). An overview can be found in Tarasov et al. (2023).

Offline goal-conditioned RL further standardizes the learning signal through goal relabeling and goal-reaching objectives, allowing comparisons between methods that span the spectrum from bootstrapped TD learning to nearly supervised representation learning (Park et al., 2025a). This builds on goal-conditioned value functions (UVFA) (Schaul et al., 2015) and hindsight relabeling (Andrychowicz et al., 2017), and connects to goal-conditioned supervised learning perspectives (Yang et al., 2022) that interpret parts of goal-reaching as near-supervised representation/behavior learning. A recent line of work in this domain focuses explicitly on non-TD objectives (Wang et al., 2023; Myers et al., 2025a;b; Zheng et al., 2025) that utilize the (quasimetric) structure of goal distances (Mohan et al., 2024).

This structure is central to our study: it lets us vary data quality systematically while holding interaction budgets fixed, and it exposes how bootstrapping-based objectives (e.g., IQ-L/HIQ-L-style backups) can change the optimization problem even when exploration is not a confounding factor.

Attribution analyses for hyperparameters. Variance-attribution methods such as fANOVA have become a standard tool for identifying which hyperparameters explain performance variability in large configuration spaces (Hutter et al., 2014). Recent tools for analyzing HPO runs make it practical to compute phase- and regime-specific importances and compare them between conditions (Segel et al., 2025). Because variance-attribution is design-dependent, several works recommend complementary analyses using fixed designs (e.g., quasi-random grids) or alternative global sensitivity measures when comparing conditions (Saltelli et al., 2008). Our use of fANOVA is aligned with this line of work, but we emphasize *phase-wise* stability under controlled dataset schedules and connect importance shifts to landscape geometry rather than treating importances in isolation.

Mechanistic diagnostics via gradients. Although prior AutoRL work documents sensitivity and nonstationarity, mechanistic explanations are less common in empirical landscape studies. Our alignment/interference measure is conceptually related to gradient conflict diagnostics in multi-task learning (Yu et al., 2020), but we apply it across relabeled goals within a single offline RL objective to connect training signals to hyperparameter landscape geometry. Our gradient interference diagnostic links objective design (bootstrapped targets versus non-TD objectives) to an observable training signal, inter-goal gradient alignment, that co-varies with landscape sharpness and phase sensitivity. This complements landscape and importance analyzes by proposing a concrete mechanism for why TD bootstrapping can amplify brittleness even when exploration is fixed.

B. Algorithmic Details

This appendix provides the precise objectives, goal-sampling procedures, and policy extraction mechanisms for the offline GCRL algorithms studied in the main text. All methods operate on a fixed offline dataset and differ primarily in how they process identical self-supervised goal signals.

B.1. Self-Supervised Goal Relabeling

Since no online interaction is permitted, all algorithms rely on self-supervised goal relabeling, where goals are sampled from states already present in the dataset. Let $\mathcal{D} = \{\tau^{(n)}\}_{n=1}^N$ denote a fixed dataset of trajectories $\tau = (s_0, a_0, s_1, \dots, s_T)$.

We consider the following goal-sampling distributions, following standard practice in offline GCRL benchmarks:

1. Uniform future-state sampling

$$p_{\mathcal{D}}^{\text{traj}}(g \mid s_t) = \text{Unif}\{s_{t'} \mid t' > t\},$$

which samples goals uniformly from future states in the same trajectory.

2. Truncated geometric future-state sampling

$$p_{\mathcal{D}}^{\text{geom}}(g \mid s_t) \propto \gamma^{t' - t}, \quad t' > t,$$

where $\gamma \in (0, 1)$ controls the decay rate and the distribution is truncated to future states within the trajectory.

3. Random-goal sampling

$$p_{\mathcal{D}}^{\text{rand}}(g),$$

which samples goals uniformly from all states in the dataset.

We also consider mixtures of these distributions.

B.2. Hierarchical Implicit Q-Learning (HIQL)

HIQL (Park et al., 2023) is a TD-based offline GCRL method that learns a goal-conditioned value function via expectile regression. The value function is parameterized as

$$V(s, g) = \tilde{V}(s, \phi(s, g)),$$

where $\phi : \mathcal{S} \times \mathcal{S} \rightarrow \mathcal{Z}$ is a state-dependent subgoal representation.

HIQL first trains V using GCIVL. From this value function, HIQL extracts two policies: a high-level policy $\pi^h : \mathcal{S} \times \mathcal{S} \rightarrow \Delta(\mathcal{Z})$ and a low-level policy $\pi^\ell : \mathcal{S} \times \mathcal{Z} \rightarrow \Delta(\mathcal{A})$, optimized via AWR-style objectives:

$$J_{\text{HIQL}}^h(\pi^h) = \mathbb{E}_{(s_t, s_{t+k}) \sim p^{\mathcal{D}}, g \sim p_{\text{mixed}}^{\mathcal{D}}(g \mid s_t)} \left[e^{\alpha(V(s_{t+k}, g) - V(s_t, g))} \log \pi^h(\phi(s_t, s_{t+k}) \mid s_t, g) \right], \quad (9)$$

$$J_{\text{HIQL}}^\ell(\pi^\ell) = \mathbb{E}_{(s_t, a_t, s_{t+1}, s_{t+k}) \sim p^{\mathcal{D}}} \left[e^{\alpha(V(s_{t+1}, s_{t+k}) - V(s_t, s_{t+k}))} \log \pi^\ell(a_t \mid s_t, \phi(s_t, s_{t+k})) \right], \quad (10)$$

where k is a subgoal hyperparameter. We omit arguments of $p^{\mathcal{D}}$ for brevity. Edge cases where $t + k$ exceeds the trajectory length are handled by truncation.

B.3. Quasimetric RL (QRL)

QRL (Wang et al., 2023) learns a quasimetric distance function $d(s, g)$ whose negative corresponds to a value function of goals in deterministic environments. QRL optimizes the constrained objective

$$\max_d \mathbb{E}_{s \sim p^D(s), g \sim p_{\text{rand}}^D(g)} [d(s, g)], \quad (11)$$

$$\text{s.t. } \mathbb{E}_{(s, s') \sim p^D(s, s')} [(d(s, s') - 1)^2] \leq \varepsilon^2, \quad (12)$$

which enforces consistency with shortest-path geometry.

In continuous-action settings, QRL also learns a latent dynamics model $f(\phi(s), a)$ and optimizes a DDPG+BC-style policy objective based on the distance learned. Both the distance function and dynamics model are trained jointly without stop-gradients. We utilize QRL implementation in Park et al. (2025a) and use Adavantage Weighted Regression (AWR) (Peng et al., 2019) for policy extraction.

C. Hyperparameters

In Table 5 we list the ranges of all hyperparameters used in the experiments on hyperparameter importance and the landscapes. We chose ranges that were substantially wider than the commonly used values. The learning rate, τ , and ϵ are logarithmically scaled due to the expectation of interesting settings in the lower region. See Section 2 for an explanation of the hyperparameters.

Hyperparameter Ranges			
Hyperparameter	Lower Bound	Upper Bound	Log Scale
Learning Rate	10^{-6}	1 or 10^{-2}	Yes
Discount Factor	0.8	0.9999	No
α	0.0	30.0	No
τ	10^{-4}	1.0	Yes
Batch Size	1	4096	No
actor_geom_sample	True	False	/
actor_p_trajgoal	0.0	1.0	No
actor_p_curgoshares	0.0	1.0	No
value_geom_sample	True	False	/
value_p_trajgoal	0.0	1.0	No
value_p_curgoshares	0.0	1.0	No
κ	0.0	1.0	No
$steps_{subgoal}$	1	500	No
ε	10^{-6}	1.0	Yes

Table 5. Hyperparameter ranges for all algorithms. The learning rate is limited to 10^{-2} for landscape analysis to zoom in on the interesting parts.

In Table 6 we list the default values for all hyperparameters. These will be used for hyperparameter response slices and gathering convergence data. They are, with a few exceptions, taken from OGBench (Park et al., 2025a).

All network architectures for value functions and policies have three hidden layers with a dimension of 512. For details, refer to OGBench (Park et al., 2025a).

D. Phased Training

To gather data during training, we apply the phased pipeline proposed by Mohan et al. (2023), as shown in Figure 4, to offline GCRL. The resulting data will allow us to study the hyperparameter landscapes throughout the training process.

First, we start training a set of configurations $C = \{\lambda^{(1)}, \lambda^{(2)}, \dots, \lambda^{(n)}\} \subseteq \Lambda$ in time steps t_0 to $t_{ls(1)}$ (ls denoting landscape), where we evaluate all configurations in C to collect landscape data. We then proceed to pick the best configuration, using its checkpoint for training in the second phase. To continue training, we start training all $\lambda \in C$ until $t_{ls(2)}$. However, instead

Hyperparameter	Hyperparameter Defaults	
	HIQL	QRL
Learning Rate	10^{-4} or 10^{-2}	10^{-4}
Discount Factor	0.99	0.99
α	3.0 (low-level and high-level)	3.0
τ	0.005	/
Batch Size	1024	1024
actor_geom_sample	False	False
actor_p_trajgoal	1.0	1.0
actor_p_curgoalshare	0.0	0.0
value_geom_sample	True	True
value_p_trajgoal	0.5	0.0
value_p_curgoalshare	0.4	0.0
κ	0.7	/
$steps_{subgoal}$	25	/
ε	/	0.05
Layer Normalization	True	True
Constant Standard Deviation	True	True
Goal Latent Dim	10	/

Table 6. Default hyperparameter values for all algorithms.

of continuing with the previous model, we use the checkpoint mentioned earlier. This ensures a fair starting point for all configurations in phase two and also implicitly schedules the hyperparameters as needed.

The process is repeated until all phases have been completed. In contrast to Mohan et al. (2023), we do not evaluate configurations by training until the last phase, as this worsens performance in our setting. Table 9 shows the change in metrics when switching from t_{phase} to t_{final} . In general, scores decrease when selecting the best-performing configurations based on t_{final} , except for HIQL on expert data, where maximum performance is higher. Landscapes appear quite similar, with slightly fewer interactions between hyperparameters for HIQL. In general, performance is lower when using t_{final} , leading us to do all experiments with $t_{ls(i)}$. This simplifies the setup and significantly reduces computational costs.

D.1. Phase Splitting

Setting phases $t_{ls(i)}$ properly is essential for gathering insights on *crucial points* in training. We do not want to set phases after our algorithm has already mostly converged but also not too early, where it is far from its potential. Knowledge about convergence is therefore essential for setting interesting phases.

We gather convergence data for one million time steps and set the target performance to 95% of the final success rate. To obtain a more stable result, we select the last intersection with the performance threshold, rather than early in the training, where performance varies the most. We will refer to this intersection as 100% training progress.

Convergence data varies across algorithms and datasets, so we collect this data for each combination separately. When we train a single agent across multiple datasets, the length of each phase is determined by the corresponding dataset’s convergence data. For data collection, we use the default hand-tuned hyperparameter configuration provided by OGBench (Park et al., 2025a). This configuration may be suboptimal for the given environment-dataset combination, leading to inaccuracies in the selected phases. Given that our primary goal is not to find the highest-performing hyperparameter configuration but rather to identify interesting time steps that roughly align across algorithms, these inaccuracies are not problematic. Note that this approach may yield phases that vary widely across algorithms or even within a single algorithm, depending on the datasets used. Gathered results should therefore not be used to compare convergence speed across algorithms or datasets, but instead to gain an understanding of hyperparameter behavior at crucial points in training.

The training curve is constructed by linearly interpolating between evaluation steps. Generally, there are more changes at the beginning, so we evaluate them more frequently. The evaluation steps divided by 1000 are:

Setting	Algorithm	Phase Transition		
		1→2	2→3	3→4
antmaze-large-0%explore	HIQL	0.137	0.344	0.342
	QRL	0.319	0.531	0.886
antmaze-large-100%explore	HIQL	0.000	0.358	0.188
	QRL	0.000	0.756	0.894
antmaze-large-40%explore	HIQL	0.067	0.736	0.719
	QRL	0.275	0.658	0.962
antmaze-large-80%explore	HIQL	0.045	0.727	0.867
	QRL	0.423	0.645	0.516
antmaze-large-scheduled	HIQL	0.000	0.000	0.514
	QRL	0.301	0.511	0.559
antmaze-medium-0%explore	HIQL	0.591	0.112	0.463
	QRL	0.091	0.741	0.960
antmaze-medium-100%explore	HIQL	0.438	0.025	0.479
	QRL	0.434	0.453	0.502
antmaze-medium-40%explore	HIQL	0.267	0.109	0.115
	QRL	0.208	0.880	0.961
antmaze-medium-80%explore	HIQL	0.378	0.131	0.523
	QRL	0.149	0.891	0.928
antmaze-medium-scheduled	HIQL	0.439	0.146	0.334
	QRL	0.256	0.306	0.944
antmaze-teleport-navigate-v0	HIQL	0.095	0.224	0.078
	QRL	0.229	0.528	0.762
humanoidmaze-medium-navigate-v0	HIQL	0.080	0.500	0.441
	QRL	0.000	0.232	0.345
pointmaze-medium-navigate-v0	HIQL	0.112	0.322	0.625
	QRL	0.869	0.779	0.831

Table 7. Optimum overlap of near-optimal hyperparameter configurations (top-10%) across consecutive training phases.

$$\{1, 2.5, 5, 7.5, 10, 20, 30, 40, 50, 75, 100, 150, 200, 300, 400, 500, 600, 700, 800, 900, 1000\}$$

Table 10 lists the training steps needed to achieve 95% performance. Low exploration noise tends to lead to faster performance convergence, especially for QRL on 0% noise.

E. fANOVA importance estimation details

This appendix documents how we compute the phase-wise hyperparameter importances shown in Figures 5 to 9.

Inputs to fANOVA. For each *phase* t , *algorithm* (QRL, HIQL), and *dataset regime* (constant mixture or scheduled data quality), we collect a set of evaluated configurations $C_t = \{(\lambda^{(i)}, f_t(\lambda^{(i)}))\}_{i=1}^{n_t}$, where $\lambda^{(i)}$ is a hyperparameter configuration and $f_t(\lambda^{(i)})$ is the corresponding phase-indexed evaluation score produced by our phased protocol (Section 3). All configurations within a phase are evaluated from the same reference checkpoint to ensure comparability.

Configuration generation (Bayesian optimization). We obtain evaluated configurations via Bayesian optimization using SMAC (through Hypersweeper), run independently per algorithm and dataset regime. We aggregate all evaluated trials from the optimization trace for the given (algorithm, dataset, phase) and pass these to DeepCAVE to compute importances. This means that the reported importance characterizes the performance variation *over the explored region of the search space induced by SMAC*, rather than over a uniform random design.

Environment	Algorithm	Exploration Ratio Transition		
		100→80	80→40	40→0
antmaze-large	HIQL	0.366	0.694	0.165
	QRL	0.052	0.533	0.831
antmaze-medium	HIQL	0.117	0.426	0.182
	QRL	0.476	0.928	0.968

Table 8. Optimum overlap of near-optimal hyperparameter configurations across exploration-ratio transitions.

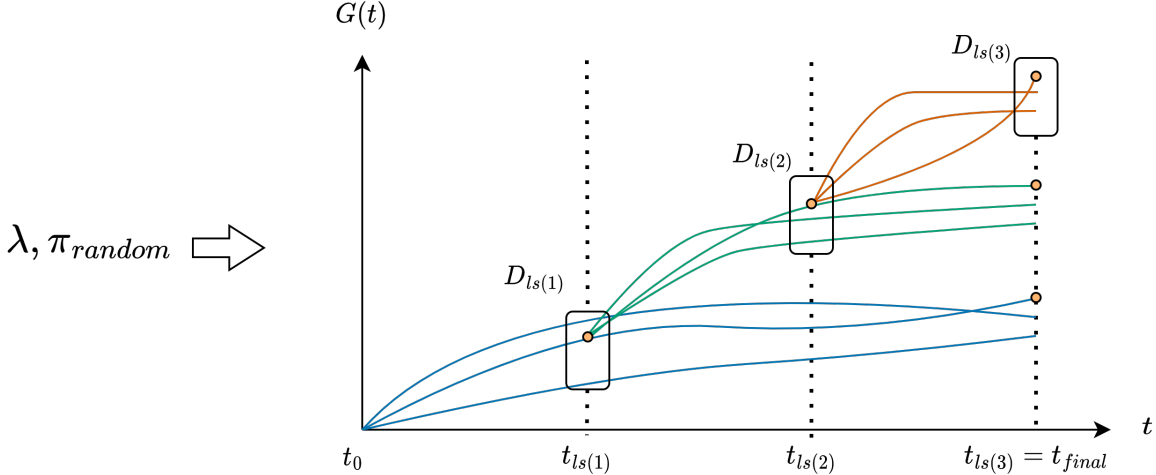


Figure 4. **Phased training** (Mohan et al., 2023). At t_0 we start training all sampled configurations and evaluate them at $t_{ls(1)}$. For the second phase, we start training from $t_{ls(1)}$, loading the checkpoint of the best configuration from phase one, and then re-evaluate all configurations at $t_{ls(2)}$. The best configuration is determined by evaluating at t_{final} , which we will set to $t_{ls(i)}$.

fANOVA computation and normalization. We compute the importances of the main-effect fANOVA as Hutter et al. (2014) as implemented in DeepCAVE. For each phase, fANOVA produces a vector of nonnegative importance $\{I_j^{(t)}\}_{j=1}^d$ in the tuned hyperparameters d , where $I_j^{(t)}$ estimates the fraction of variance in $f_t(\lambda)$ attributable to the hyperparameter j (marginalizing over the other hyperparameters under the empirical design distribution). We report normalized importances such that $\sum_j I_j^{(t)} = 1$ within each phase.

Phases and scheduled data quality regime. In the scheduled data quality setting, the phases correspond to the fixed mixtures of the dataset $100\% \rightarrow 80\% \rightarrow 40\% \rightarrow 0\%$ to explore, as described in Section 3. Each phase is trained and evaluated under its corresponding mixture; importances are computed separately per phase.

Stability and concentration summaries. In the main text, we summarize phase-wise importance profiles using: (i) concentration statistics (Top- k importance mass) and (ii) stability statistics across phases (rank similarity across consecutive phases). These diagnostics compress the full profiles shown below into quantities that align with our benignness claims.

E.1. Phase-wise fANOVA profiles under scheduled data quality

F. Hyperparameter Landscape Construction and Analysis

F.1. Phase selection

To ensure that hyperparameter landscapes are evaluated at comparable points in training across algorithms and data regimes, we define phase boundaries based on algorithm- and dataset-specific convergence behavior. For each algorithm and dataset regime, we train a reference agent for a fixed budget of 10^6 environment steps and record its evaluation performance.

Configuration Evaluation at Final Time Step

Algorithm	Setting	Epsilon Optimality		Mean	Max
		> 0.9 Ratio	> 0.8 Ratio		
HIQL	40% Noise	-0.02	-0.02	-0.02	-0.01
	0% Noise	0.01	0.01	0.05	0.11
QRL	40% Noise	-0.06	-0.04	-0.02	-0.01
	0% Noise	-0.24	-0.11	-0.06	-0.01

Table 9. Change in metrics when switching from $t_{ls(i)}$ to t_{final} . Evaluated on Learning Rate and Discount Factor for 0% Noise and 40% Noise on antmaze-medium-v0. Aggregated over all phases. t_{final} is the last time step of the last phase.

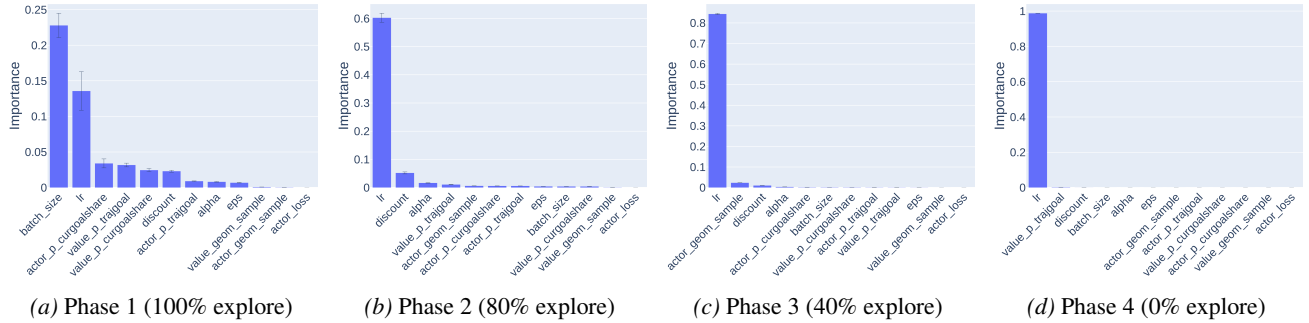


Figure 5. **QRL:** Phase-wise fANOVA main-effect importances under scheduled data quality for antmaze-medium-v0.

We define 100% training progress as the *last* time step at which the evaluation metric exceeds 95% of the final observed performance. Using the last intersection, rather than the first, avoids early transient effects and yields a more stable phase placement. The phase boundaries $t_{ls(i)}$ are then set as fixed fractions of this progress.

Because convergence behavior varies across algorithms and dataset regimes, phase lengths may differ substantially. As a result, phase indices should not be interpreted as indicators of relative convergence speed, but rather as anchors for analyzing hyperparameter behavior at comparable stages of learning.

F.2. Hyperparameter spaces and configuration sampling

Let Λ denote the hyperparameter space associated with a given algorithm. Each Λ includes algorithm-specific parameters (e.g., learning rates, regularization coefficients, discount factors) as well as shared optimization parameters. Continuous dimensions are bounded and sampled on appropriate scales (e.g., log-uniform for learning rates), while discrete parameters are sampled uniformly.

For each algorithm, we sample a fixed configuration set $C = \{\lambda^{(1)}, \dots, \lambda^{(N)}\} \subseteq \Lambda$ prior to training. The same configuration set is reused across all data regimes and phases to enable direct comparison of landscape geometry. Configuration sampling is performed once and maintained fixed throughout the study.

The exact hyperparameter ranges and sampling distributions for each algorithm are listed in Table 5.

F.3. Landscape datasets and checkpoint resets

For each phase i , all configurations $\lambda \in C$ are trained starting from a shared reference checkpoint, corresponding to the configuration that performs best in phase $i - 1$ under the same algorithm and data regime. This reset rule ensures that landscape measurements reflect the *local* effect of hyperparameters within each phase, rather than cumulative differences from earlier training.

Evaluating each configuration at $t_{ls(i)}$ yields a landscape dataset

$$D_{ls}^{(i)} = \{(\lambda^{(j)}, f_i(\lambda^{(j)}))\}_{j=1}^N,$$

95% Performance Threshold			
Algorithm	Environment	Exploration Noise	Training Steps
HIQL	antmaze-medium-v0	0%	99734
		40%	191653
		80%	757083
		90%	894143
		100%	669361
QRL	antmaze-medium-v0	0%	18461
		40%	323333
		80%	308714
		90%	188812
		100%	723214
HIQL	antmaze-large-v0	0%	321818
		40%	747500
		80%	633999
		100%	995000
QRL	antmaze-large-v0	0%	64750
		40%	967777
		80%	750000
		100%	895000
HIQL	pointmaze-medium-v0	0%	23142
QRL	pointmaze-medium-v0	0%	971562
HIQL	antmaze-teleport-v0	0%	25714
QRL	antmaze-teleport-v0	0%	620714
HIQL	humanoidmaze-medium-v0	0%	390000
QRL	humanoidmaze-medium-v0	0%	843333

Table 10. Training steps required to achieve 95% performance for each algorithm and setting combination. Performance is measured using success rate, because it is the measure the agent is trained on. Data was collected using hand-tuned configurations per algorithm.

where $f_i(\lambda)$ denotes the aggregated evaluation metric in random seeds. Unless otherwise stated, the evaluation metrics correspond to the success rate averaged over K evaluation episodes.

F.4. Landscape modeling and visualization

To visualize two-dimensional slices of the hyperparameter landscapes, we follow (Mohan et al., 2023) and fit independent Gaussian process regressors (IGPRs) to the observed configuration–performance pairs. Each IGPR is trained on a pair of selected hyperparameters, marginalizing over all others.

We emphasize that IGPRs are used *only* for visualization and qualitative inspection of landscape shape. All quantitative metrics reported in the main paper are computed directly on the evaluated configurations without reliance on surrogate predictions.

Hyperparameter importance and interactions. We compute phase-dependent hyperparameter importances using fANOVA (Hutter et al., 2014) via DeepCAVE (Segel et al., 2025). This yields marginal importance scores for individual hyperparameters as well as interaction mass capturing higher-order effects. To quantify changes in importance profiles across phases, we computed cosine distance between phase-wise importance vectors.

F.5. Reproducibility details

All experiments are conducted with fixed random seeds per configuration and multiple evaluation rollouts. Compute budgets, seed counts, and implementation details are reported alongside hyperparameter tables. The code for landscape construction, analysis, and visualization will be released upon publication.

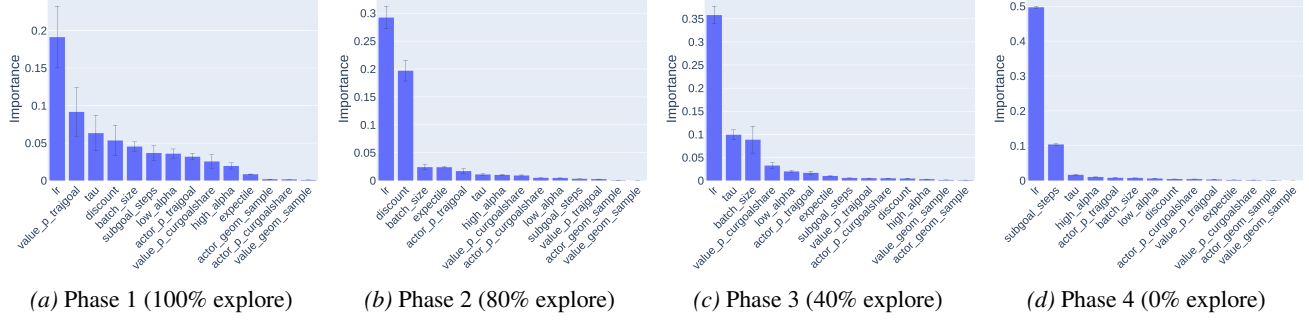


Figure 6. HIQL: Phase-wise fANOVA main-effect importances under scheduled data quality for antmaze-medium-v0.

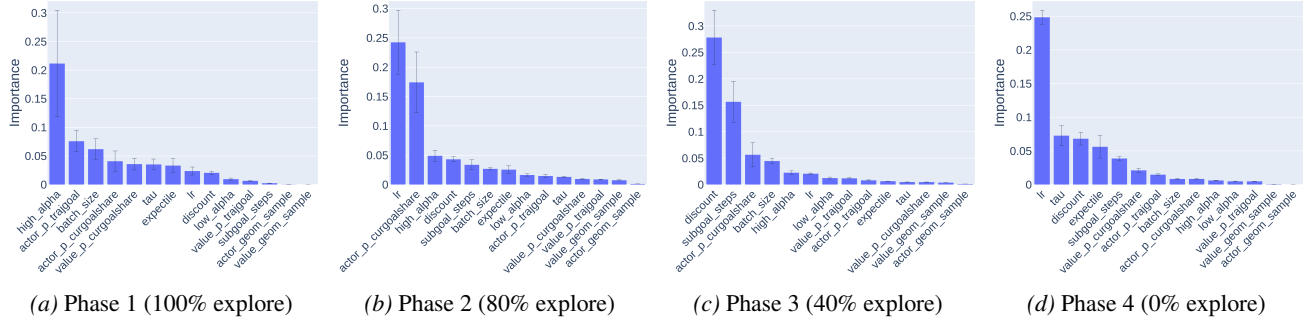


Figure 7. HIQL: Phase-wise fANOVA main-effect importances under scheduled data quality for antmaze-large-v0.

F.6. Phase Mobility Plots

Phase mobility of near-optimal hyperparameters. We visualize how the optimal region shifts across training phases and data regimes. For each setting (scheduled or constant), we identify the "near-optimal" region as the set of hyperparameters achieving the top 10% of performance within that specific phase. We plot these regions in the learning rate–discount factor plane. Under constant data quality, QRL exhibits relatively stable near-optimal regions across phases. In contrast, HIQL shows pronounced mobility, with the optimal region shifting significantly between early and late phases, indicating a greater sensitivity to the training stage and TD bootstrapping dynamics.

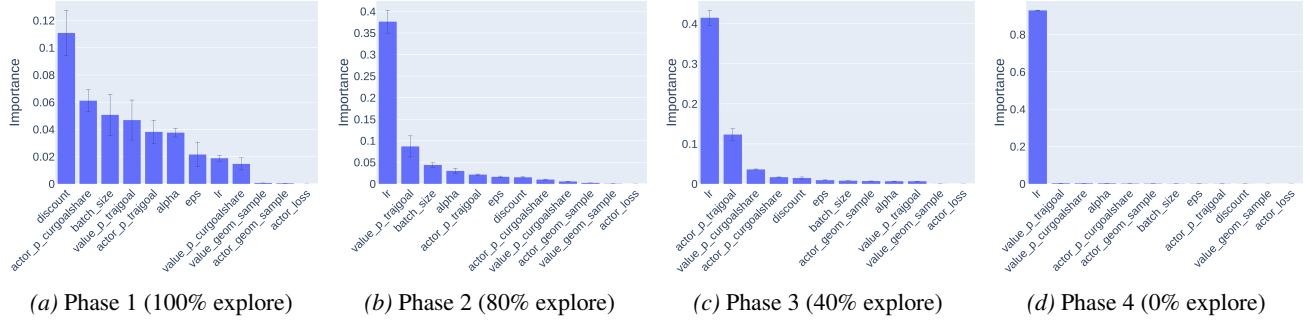


Figure 8. **QRL**: Phase-wise fANOVA main-effect importances under scheduled data quality for antmaze-large-v0.

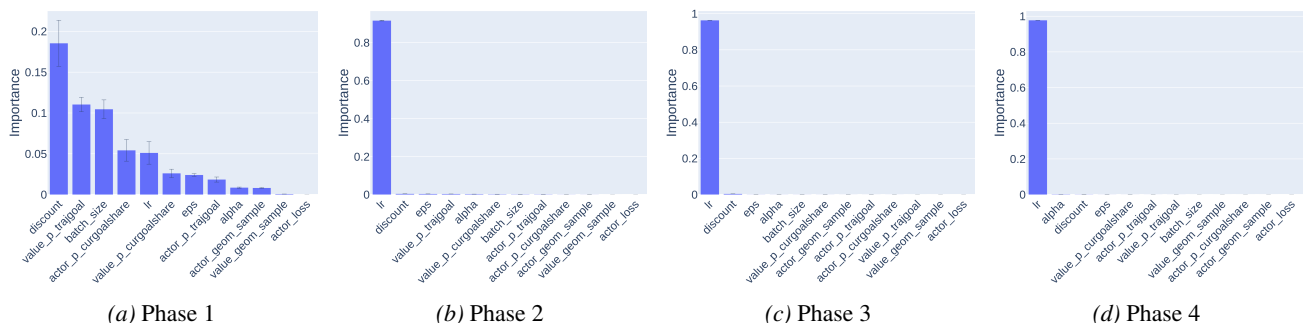


Figure 9. **QRL**: Phase-wise fANOVA main-effect importances under expert data quality for antmaze-medium-v0.

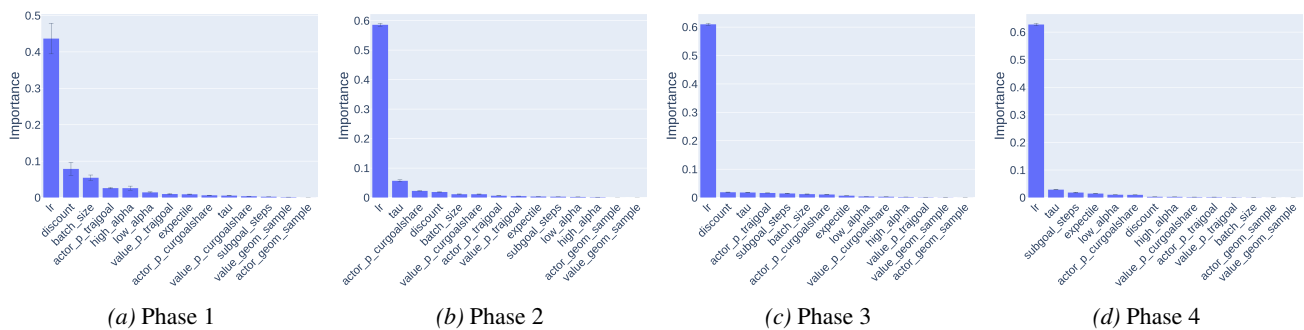


Figure 10. **HIQL**: Phase-wise fANOVA main-effect importances under expert data quality for antmaze-medium-v0.

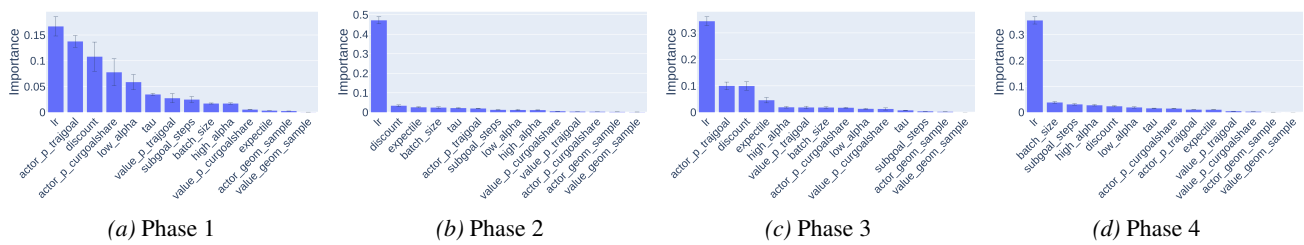


Figure 11. **HIQL**: Phase-wise fANOVA main-effect importances under expert data quality for antmaze-large-v0.

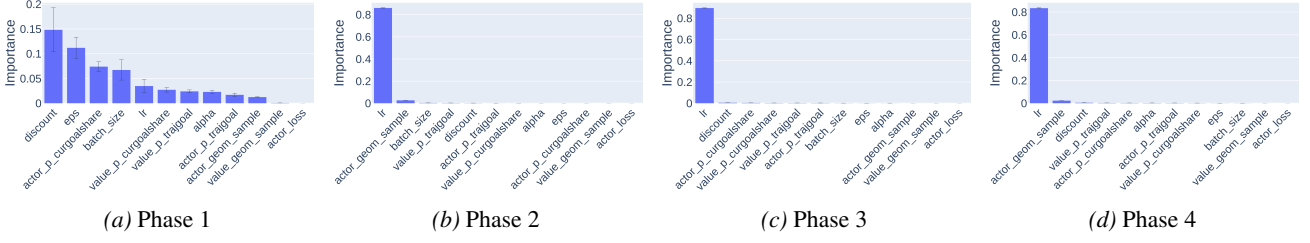


Figure 12. QRL: Phase-wise fANOVA main-effect importances under expert data quality for antmaze-large-v0.

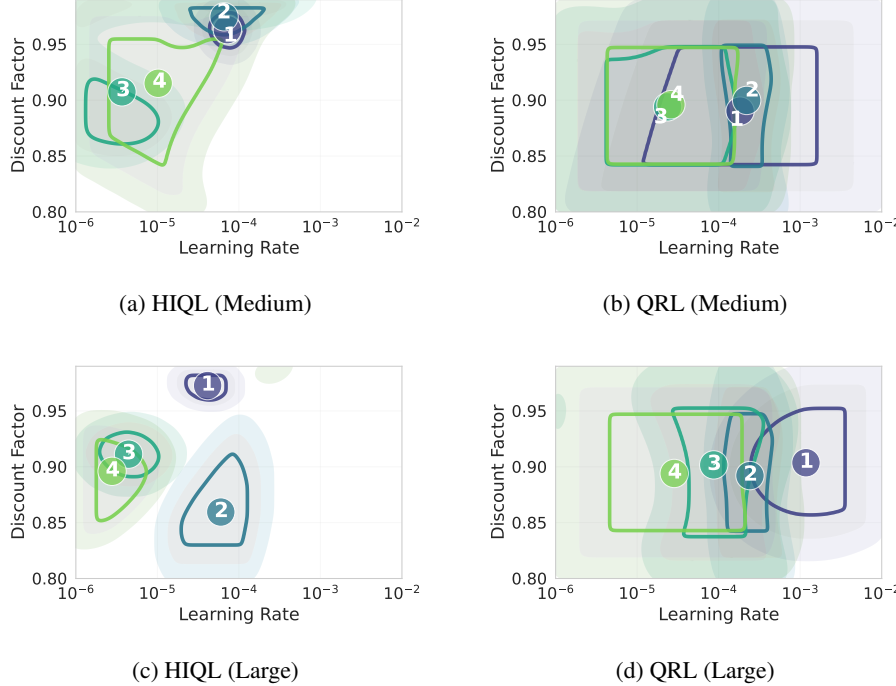


Figure 13. Scheduled noise mobility plots across maze scales. We illustrate the sensitivity of learning objectives to scheduled training phases where data quality improves over time. **Top:** Mobility results for the antmaze-medium-v0 environment across transition phases. **Bottom:** Results for the antmaze-large-v0 environment. Note how the stability of the near-optimal region in the learning-rate – discount-factor plane varies between the bootstrapped HIQL and the representation-based QRL.

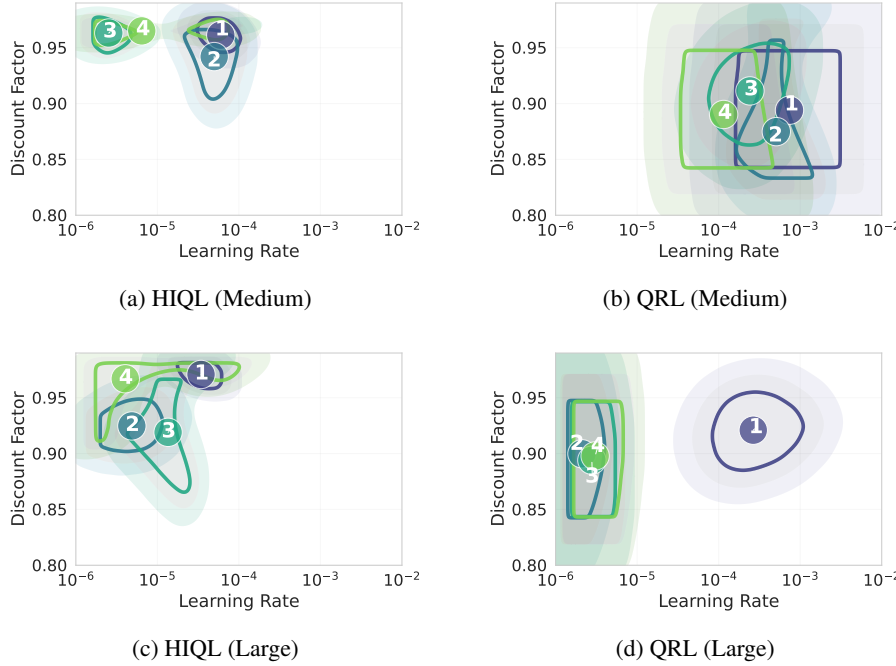


Figure 14. Pure exploration noise mobility plots. **Top:** Mobility results for the antmaze-medium-v0 environment. **Bottom:** Mobility results for the antmaze-large-v0 environment. Similar to the scheduled noise experiments, the representation learning method (QRL) maintains a more stable optimal hyperparameter region compared to the bootstrapped method (HIQL) even under exploration noise.

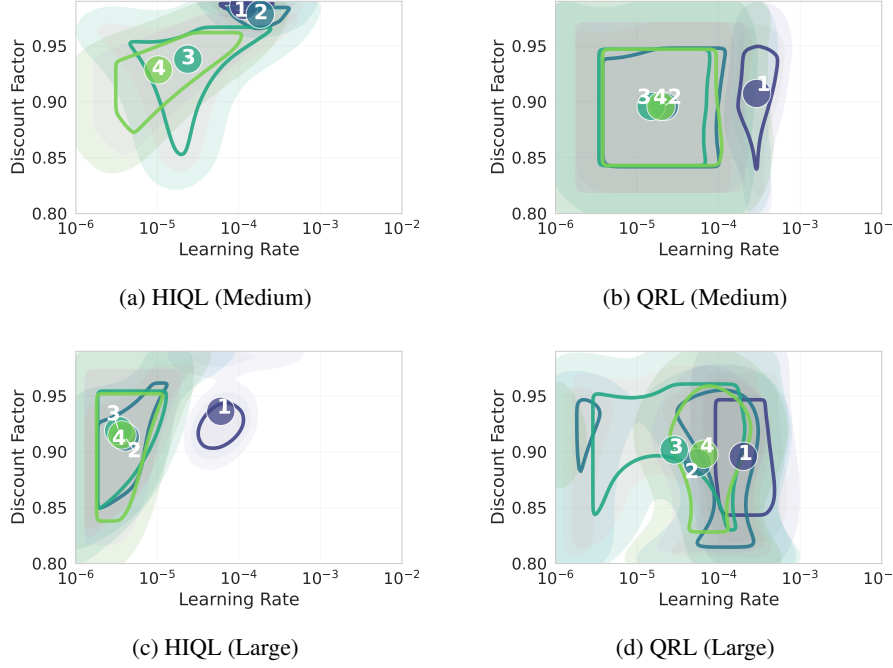


Figure 15. 80% noise mobility plots. Visualization of hyperparameter landscape stability under high-noise conditions. **Top:** Mobility results for the antmaze-medium-v0 environment with 80% exploration noise. **Bottom:** Mobility results for the antmaze-large-v0 environment. These plots demonstrate how the near-optimal region shifts or remains anchored when the dataset is dominated by sub-optimal exploration transitions.

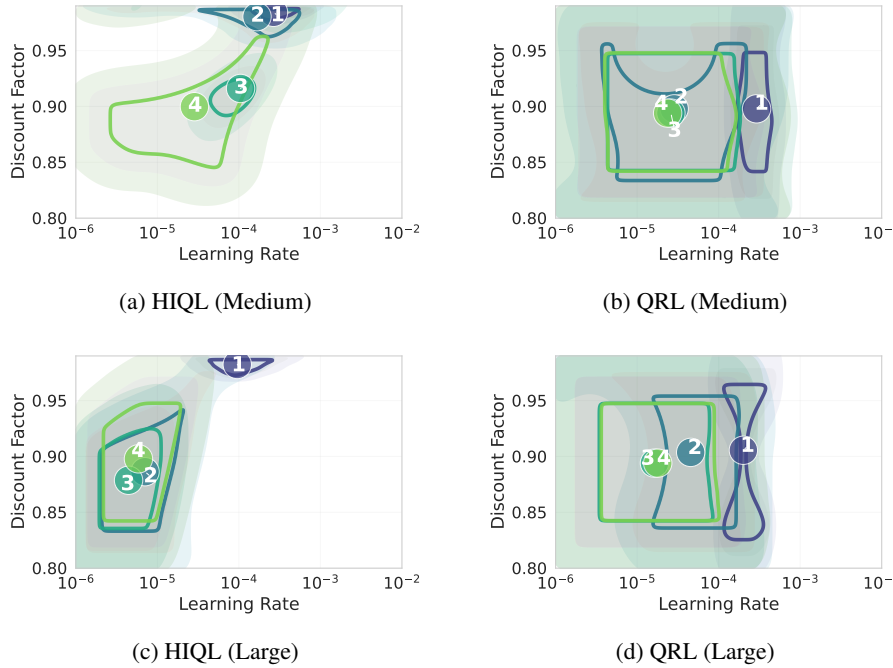


Figure 16. 40% noise mobility plots. Hyperparameter sensitivity visualization for intermediate data quality levels. **Top:** Results for the antmaze-medium-v0 environment with 40% noise. **Bottom:** Results for the antmaze-large-v0 environment. At this intermediate noise level, we can observe the transition of the optimal hyperparameter region as the dataset becomes increasingly dominated by goal-directed navigation data.

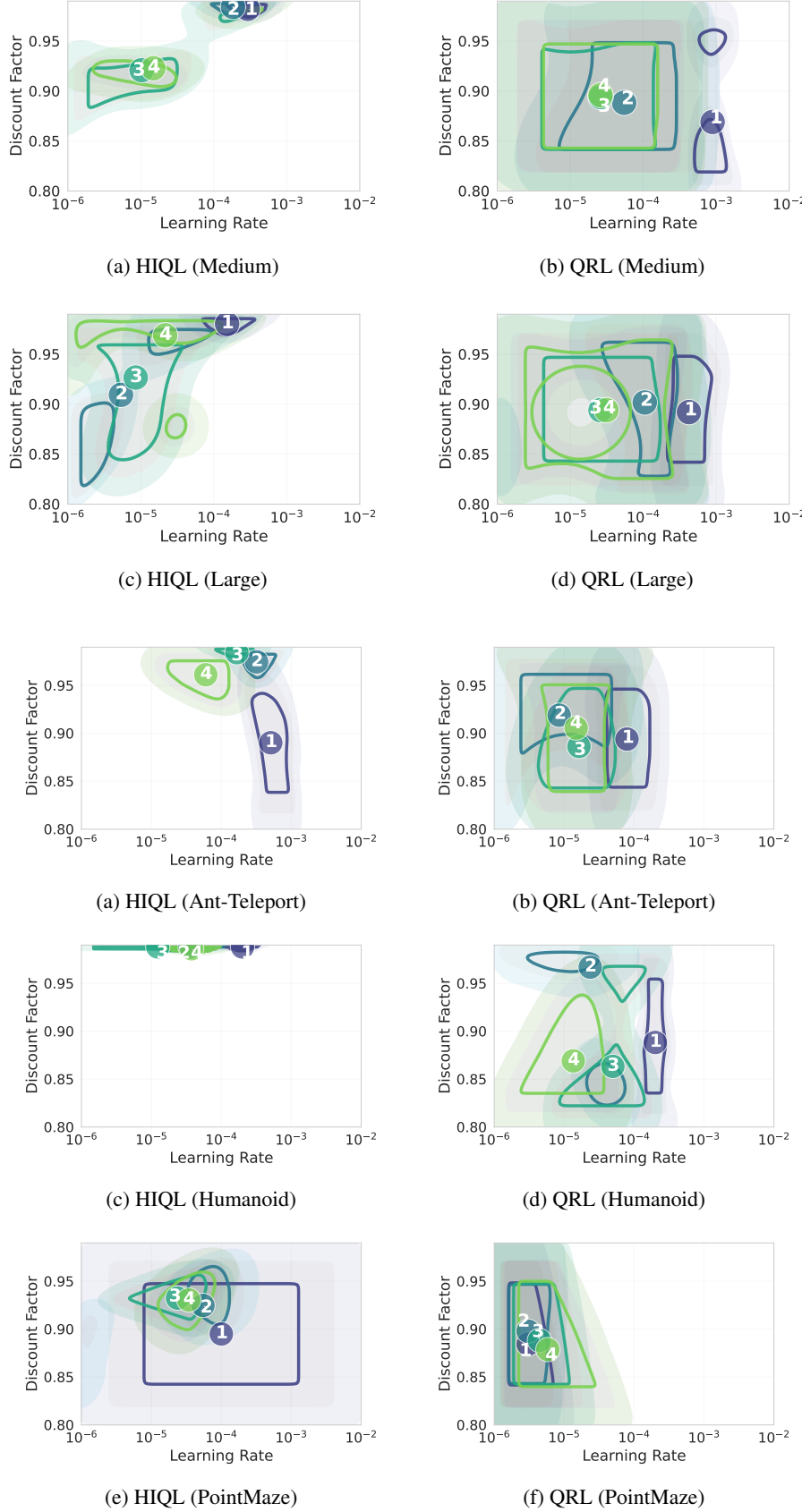


Figure 17. Pure expert data mobility plots. Visualization of the hyperparameter landscape using high-quality navigation data without exploration noise. **Top:** Results for the `antmaze-medium-v0` environment. **Bottom:** Results for the `antmaze-large-v0` environment. This setup represents the cleanest data regime, allowing for a direct comparison of how HIQL and QRL perform when the data quality is near-optimal.

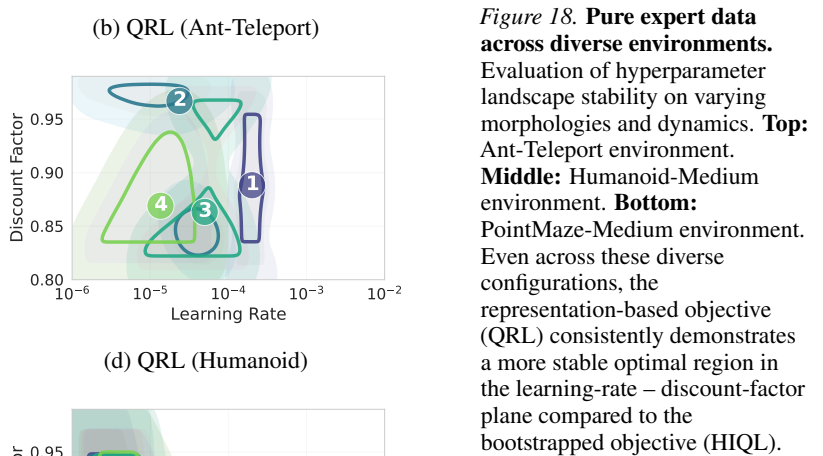


Figure 18. Pure expert data across diverse environments. Evaluation of hyperparameter landscape stability on varying morphologies and dynamics. **Top:** Ant-Teleport environment. **Middle:** Humanoid-Medium environment. **Bottom:** PointMaze-Medium environment. Even across these diverse configurations, the representation-based objective (QRL) consistently demonstrates a more stable optimal region in the learning-rate – discount-factor plane compared to the bootstrapped objective (HIQL).

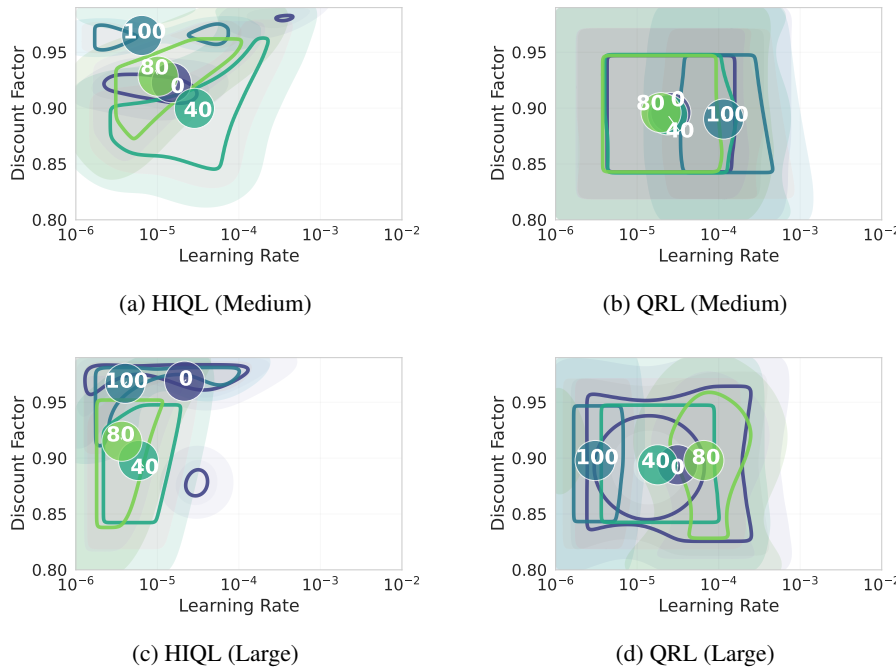


Figure 19. Mobility plots across data quality levels for the final training phase. We visualize how the optimal hyperparameter region drifts when evaluating the last phase of training across different data mixtures. **Top:** Results for antmaze-medium-v0. **Bottom:** Results for antmaze-large-v0. These plots isolate the learning mechanism’s sensitivity to the final data distribution, highlighting the contrast between the stability of the representation-learning objective (QRL) and the shifting landscape of the bootstrapped objective (HIQL).